A cell surface *O*-glycosylated peptide, AGP21, acts on the brassinosteroid pathway and modulates root hair cell fate

Cecilia Borassi[1,#], Javier Gloazzo Dorosz[1,#,*], Martiniano M. Ricardi[2,#,**], Laercio Pol Fachin[3], Mariana Carignani Sardoy[1], Eliana Marzol[1], Silvina Mangano[1], Diana Rosa Rodríguez Garcia[1], Javier Martínez Pacheco[1], Yossmayer del Carmen Rondón Guerrero[1], Silvia M. Velasquez[1,***], Bianca Villavicencio[4], Marina Ciancia[5], Georg Seifert[6], Hugo Verli[4] & José M. Estevez[1,7,†]

[1]Fundación Instituto Leloir, Av. Patricias Argentinas 435, Buenos Aires CP C1405BWE, Argentina.
[2]Instituto de Fisiología, Biología Molecular y Neurociencias (IFIByNE-CONICET), Departamento de Fisiología y Biología Molecular y Celular (FBMC), Facultad de Ciencias Exactas y Naturales, Universidad de Buenos Aires C1428EGA, Argentina.
[3]Centro Universitário CESMAC, Maceió, Brazil.
[4]Centro de Biotecnologia, Universidade Federal do Rio Grande do Sul CP 15005, Porto Alegre 91500-970 RS, Brazil.
[5]Universidad de Buenos Aires, Facultad de Agronomía, Departamento de Biología Aplicada y Alimentos, Cátedra de Química de Biomoléculas, Buenos Aires, Argentina and CONICET-Universidad de Buenos Aires, Centro de Investigación de Hidratos de Carbono (CIHIDECAR), Buenos Aires, Argentina.
[6]University of Natural Resources and Life Science, BOKU Vienna, Department of Applied Genetics and Cell Biology, Muthgasse 11 A-1190, Vienna, Austria.
[7]Centro de Biotecnología Vegetal (CBV), Facultad de Ciencias de la Vida, Universidad Andrés Bello, Santiago, Chile.

[#]co-first authors
[†]Correspondence should be addressed. Email: jestevez@leloir.org.ar

Word count 3,399

[*] Current address: Grupo de Investigación Interdisciplinario en Ciencias Naturales, Colegio Gimnasio Vermont, 111166 Bogotá, Colombia.
[**] Current address: Developmental Genetics, University of Tübingen, 72076 Tübingen, Germany.
[***]Current address: University of Natural Resources and Life Science, BOKU Vienna, Department of Applied Genetics and Cell Biology, Muthgasse 11 A-1190, Vienna, Austria.

Highlights

- **Perturbation of AGPs and the loss of AGP21 peptide trigger an abnormal RH cell fate.**

- **AGP21-mediated repression of *GL2* expression activates the expression of RSL4 and EXP7 root hair proteins.**

- **AGP21 peptide acts in both a BR-dependent and BR-independent manner, with both pathways converging on a BIN2 downstream signalling cascade to controls *GL2* expression.**

Summary

Root hairs (RHs) develop from specialized epidermal cells called trichoblasts, whereas epidermal cells that lack RHs are known as atrichoblasts. The mechanism controlling root epidermal cell fate is only partially understood. Root epidermis cell fate is regulated by a transcription factor complex that promotes the expression of the homeodomain protein GLABRA 2 (GL2), which blocks RH development by inhibiting ROOT HAIR DEFECTIVE 6 (RHD6). Suppression of GL2 expression activates RHD6, a series of downstream TFs including ROOT HAIR DEFECTIVE 6 LIKE-4 (RSL4 [Yi et al. 2010]) and their target genes, and causes epidermal cells to develop into RHs. Brassinosteroids (BRs) influence root epidermis cell fate. In the absence of BRs, phosphorylated BIN2 (a Type-II GSK3-like kinase) inhibits a protein complex that directly downregulates GL2 [Chen et al. 2014]. Here, we demonstrate that the genetic and pharmacological perturbation of the arabinogalactan protein (AGP) AGP21 in *Arabidopsis thaliana*, triggers aberrant RH development, similar to that observed in plants with defective BR signaling. We reveal that an *O*-glycosylated AGP21 peptide, which is positively regulated by BZR1, a transcription factor activated by BR signaling, affects RH cell fate by altering *GL2* expression in a BIN2-dependent manner. These results indicate that perturbation of a cell surface AGP disrupts BR perception and inhibits the downstream effect of BIN2 on the RH repressor GL2 in root epidermal cells. In addition, AGP21 also acts in a BR-independent, AGP-dependent mode that together with BIN2 signalling cascade controls RH cell fate.

Word count 241

Introduction

Plant roots not only anchor the plant into the soil but allow them to absorb water and nutrients from the soil. Root hairs (RHs) are single cell protrusions developed from the epidermis that increase the root surface area exposed to the soil enhancing water and nutrients uptake. Many factors determine whether, or not, an epidermal cell will develop into a RH. These factors include both, environmental cues (such as nutrients in the soil) and signals from the plant itself, such as hormones like brassinosteroids (BRs), ABA, ethylene and auxin (Van Hengel et al. 2004; Masucci and Schiefelbein 1994, 1996; Kuppusamy et al., 2009). RH cell fate in the model plant *Arabidopsis* is controlled by a well-known developmental program, regulated by a complex of transcription factors composed by WEREWOLF (WER)-GLABRA3 (GL3)/ENHANCER OF GLABRA3 (EGL3)-TRANSPARENT GLABRA1 (TTG1) that promotes the expression of the homeodomain protein GLABRA 2 (GL2) (Ryu et al. 2005; Song et al. 2011; Schiefelbein et al. 2014; Balcerowicz et al. 2015), which ultimately blocks the root hair pathway by inhibiting ROOT HAIR DEFECTIVE 6 (RHD6) (Lin et al. 2015). The suppression of GL2 expression triggers epidermal cells to enter into the root hair cell fate program by the concomitant activation of RHD6 and a well-defined downstream gene network. As a consequence, RH and non-RH cell files are patterned alternately in rows within the root epidermis. In trichoblasts, a second transcription factor complex composed by CAPRICE (CPC)-GL3/EGL3-TTG1 suppresses GL2 expression (Schiefelbein et al. 2014), forcing cells to enter the RH cell fate program via concomitant RHD6 activation and downstream TFs, including RSL4, and RH genes (Yi et al. 2010). The plant steroid hormones, BRs play essential roles in regulating many developmental processes (Savaldi-Goldstein et al., 2007; 2010; Hacham et al., 2011; Yang et al., 2011). BRs are perceived by the receptor kinase BRASSINOSTEROID INSENSITIVE 1 (BRI1) (Li & Chory, 1997; Hothorn et al., 2011; She et al., 2011). One of the BRI1 substrate, BR-SIGNALING KINASE (BSK), transduces the BR signaling through *bri1* SUPPRESSORS 1 (BSU1) to inactivate a GSK3-like kinase BRASSINOSTEROID INSENSITIVE 2 (BIN2), which triggers high levels of the dephosphorylated form of transcriptional factors BRI1 EMS SUPPRESSOR 1 (BES1)/BRASSINAZOLE RESISTANT 1 (BZR1) in the nucleus to regulate gene expression (Yan et al. 2009; Yang et al., 2011). In recent years, a molecular mechanism was proposed by which BR signaling controls RH cell fate by inhibiting BIN2 phosphorylation activity to modulate *GL2* expression (Chen et al. 2014). In atrichoblasts, BIN2 phosphorylates TTG1, controlling protein complex TTG1-WER-GL3/EGL3 activity, and stimulating *GL2* expression (Chen et al. 2014).

Plant cell surface proteoglycans known as arabinogalactan proteins (AGPs) function in a broad developmental processes such as cell proliferation, cell expansion, organ extension, and somatic embryogenesis (Tan et al. 2004; Seifert & Roberts 2007; Pereira et al. 2015; Ma et al. 2018). The precise mechanisms underlying AGP action in these processes are completely unknown (Ma et al. 2018). AGP peptides are post-translationally modified in the ER-Golgi, undergoing signal peptide (SP) removal, proline-hydroxylation/Hyp-*O*-glycosylation, and C-terminal GPI anchor signal (GPI-AS) addition (Schultz et al. 2004; Ma et al. 2018). Processed mature AGP-peptides are 10–13 amino acids long and bear few putative *O*-glycosylation sites (*O*-AG). Few prolines in the AGP

122 peptides are hydroxylated *in vivo* as Hyp (Hyp=O), suggesting that AGP peptides are *O*-
123 glycosylated at maturity (Schultz et al. 2004). All these posttranslational modifications make the
124 study of AGPs very complex with almost no defined biological functions of any individual AGP
125 (Ma et al. 2018). Interestedly, in this work we have identified that disruption of plant specific
126 AGPs, and in particular of a single *O*-glycosylated AGP peptide (AGP21), interfere in a specific
127 manner with BR perception and BIN2 downstream effect on the repression of RH development.
128 We have found that an *O*-glycosylated AGP21-peptide positively regulated by the BR transcrip-
129 tion factor BZR1, impacts on RH cell fate by controlling GL2 expression. The molecular mecha-
130 nism proposed here for AGP21-regulated RH cell fate could be possibly extrapolated to other
131 developmental regulated programs that are under the control of the BR pathway (e.g. xylem and
132 phloem differentiation, pro-cambium fate, etc).
133
134 **Results and Discussion**
135
136 **AGP perturbation influences root hair (RH) cell fate programming**
137 To determine whether *O*-glycosylated AGPs regulate specific RH developmental processes, we
138 exposed roots of *Arabidopsis thaliana* to β-glucosyl Yariv (β-Glc-Y), which specifically binds struc-
139 tures in the *O*-glycans of AGPs: oligosaccharides with at least 5–7 units of 3-linked *O*-galactoses
140 (Yariv et al. 1967; Kitazawa et al. 2013). β-Glc-Y–linked AGP complexes on the cell surface induce
141 AGP aggregation and disrupt native protein distribution, triggering developmental reprogram-
142 ming (Guan & Nothnagel 2004; Sardar et al. 2006). α-mannosyl Yariv (α-Man-Y), an analog that
143 does not bind to AGPs, served as the control. While α-Man-Y treatment did not affect RH cell
144 fate (≈2–5% of total RHs that are contiguous), β-Glc-Y treatment increased contiguous RH devel-
145 opment (≈30-40%) (**Figure S1A**), suggesting that *O*-glycosylated AGPs influence RH formation.
146
147 To test whether *O*-glycans on hydroxyproline-rich glycoproteins (HRGPs) alter RH cell fate, we
148 blocked proline 4-hydroxylase enzymes (P4Hs) that catalyse proline (Pro)-hydroxylation into hy-
149 droxyl-proline units (Hyp), the subsequent step of HRGP *O*-glycosylation (Velasquez et al. 2011,
150 2015a). Two P4H inhibitors, α,α-dipyridyl (DP) and ethyl-3,4-dihydroxybenzoate (EDHB), prevent
151 Pro-hydroxylation (Barnett 1970; Majamaa et al. 1986); both increased contiguous RH develop-
152 ment to ≈15–20% (**Figure S1B**). Additionally, *p4h5* (a key P4H in roots [Velasquez et al. 2011;
153 2015a]) and four glycosyltransferase mutants defective in AGP *O*-glycosylation (*hpgt* triple mu-
154 tant*; ray1*, *galt29A*, and *fut4 fut6*) (see **Table S1**) showed significantly increased (≈8–20%) ec-
155 topic RH development (**Figure 1A**), substantiating the previous report that the triple mutant
156 *hpgt* mutant has an increased RH density (Ogawa-Ohnishi & Matsubayashi 2015). These mutants
157 were mostly insensitive to β-Glc-Y; however, the treatment increased the number of contiguous
158 RHs in *fut4 fut6,* although to a lesser extent than in the wild type (**Figure 1B**). β-Glc-Y inhibits
159 root cell expansion (Willats & Knox 1996; Ding & Zhu 1997). Glycosyltransferase (GT) mutations
160 affecting extensin (EXTs) *O*-glycosylation (e.g. *rra3* and *sgt1 rra3*; **Table S1**) drastically affect RH
161 cell elongation (Velasquez et al. 2015b). Intriguingly, these mutations did not affect RH cell fate,
162 and β-Glc-Y stimulated ectopic RH development, indicating that EXT O-glycosylation does not

163 function in RH cell fate reprogramming (**Table S1**, **Figure 1C**), and specifically *O*-glycans attached
164 to AGPs do. *P4H5* and *AGP-related GTs (e.g. RAY1, GALT29A, HPGT1-HPGT3* and *FUT4/FUT6),* are
165 expressed in the root epidermis elongation and differentiation zones (**Supplementary Item 1**).
166 Under-arabinosylated AGPs in *ray1* and under–*O*-fucosylated AGPs in *fut4 fut6* show similar root
167 growth inhibition (Liang et al. 2013; Trypona et al. 2014), highlighting a key role for AGP *O*-
168 glycans in regulating root cell development, albeit by unknown mechanisms.
169
170 **The BR–BZR1 pathway regulates AGP21 expression**
171 Brassinosteroid (BR) signaling regulates RH cell patterning (Cheng et al. 2015). The BR-insensitive
172 mutant, *bri1-116*, developed many (≈20%) contiguous RH cells (**Supplementary Item 2A**),
173 resembling plants subjected to β-Glc-Y and DP/EDHB treatments (**Figure S1**). The *agp21*, *p4h5*,
174 *hpgt* triple mutant, *ray1-1*, *galt29A*, and *fut4 fut6* mutants exhibited similar phenotypes,
175 suggesting that interplay between cell surface AGPs and BR signaling determines RH cell fate. As
176 chromatin-immunoprecipitation (ChIP)-sequencing and RNA-sequencing indicate that BZR1
177 directly upregulates *AGP* expression, most predominantly *AGP21* (Sun et al. 2010), we
178 investigated how root epidermal BR signaling regulates *AGP21* expression. Since the *AGP21*
179 regulatory region contains one BZR1 binding motif (E-BOX, CATGTG at -279 bp relative to ATG
180 start codon), we tested whether BR directly modulates *AGP21* expression. Compared with no
181 treatment, 100 nM BL (brassinolide, BR's most active form) enhanced of both AGP21p::GFP
182 (transcriptional reporter) and AGP21p::V-AGP21 (V= Venus tag; translational reporter)
183 expression (**Supplementary Item 2B–C**). Expression of *AGP21p::GFP* in *bri1-116* resulted in lower
184 *AGP21* expression than in untreated wild type (**Supplementary Item 2B**), confirming that BR-
185 mediated BZR1 controls *AGP21* expression in the root.
186
187 Trichoblasts and atrichoblasts expressed V-AGP21 peptide in a discontinuous pattern
188 (**Figure S1C**), indicating that some root epidermal cells lacked AGP21. Treatment with β-Glc-Y—
189 but not α-Man-Y—resulted in excess AGP21p::Venus-AGP21 at transverse cell walls (**Figure S1C**).
190 We used the BZRp::BZR1-YFP reporter to test whether disrupting PM AGPs with β-Glc-Y would
191 downregulate the response to BL (**Supplementary Item 3A**). Treatment with 100 nM BL induced
192 *BZR1* expression, whereas exposure to β-Glc-Y or β-Glc-Y followed by 100 nM BL suppressed
193 *BZR1* expression, suggesting that AGP disruption affects BR perception and downstream BZR1-
194 mediated signaling. However, global BR–BZR1/BES1-mediated transcriptional responses are not
195 involved in the anomalous RH cell fate phenotype, because lines constitutively expressing BZR1
196 (BZR1-D) and BES1 (BES1-D), overexpressing BZR1 and BES1 lines, and CRISPR-CAS9 null *bzr1* and
197 *bes1* mutants showed no anomalous phenotypes (**Supplementary Item 3B)**.
198
199 ***O*-glycosylated AGP21 peptide influences RH cell fate**
200 The molecular link to BR–BRZ1 signaling suggested that AGP21 function in RH cell fate
201 determination. The AGP21 deficient mutant *agp21* (**Supplementary Item 4A–B**), exhibited
202 ectopic contiguous RHs (**Figure 2B**). Both *AGP21* expression under its endogenous promoter
203 (*AGP21p::V-AGP21/agp21*) and overexpression (*35Sp::V-AGP21/agp21*) restored a wild type RH

204 phenotype and patterning to *agp21* (**Figure 2B**), confirming that deficient *AGP21* expression
205 causes contiguous RH development. Furthermore, while β-Glc-Y treatment triggered up to ≈30-
206 40% of contiguous RH (vs. ≈2–5% induced by α-Man-Y) in the wild type (**Figure S1**), it induced no
207 additional anomalous RH in *agp21* (vs. α-Man-Y treatment or untreated roots) (**Figure 2B**). We
208 tested whether the closely related BZR1-induced peptide AGP15 functions with AGP21. *agp15*
209 (**Supplementary Item 4C–D**) exhibited a milder phenotype than *agp21*, and the double
210 *agp15 agp21* double mutant had no additional effects to *agp21* (**Supplementary Item 4E**).
211 Together, these results confirm that β-Glc-Y acts through *O*-glycosylated AGP21 to stimulate
212 contiguous RH development.
213
214 **RH cell fate determination requires *O*-glycosylation of the AGP21 peptide**
215 To determine whether functional AGP21 requires *O*-glycosylation, three putative *O*-glycosylation
216 sites were mutated (Pro→Ala) (**Figure 2A**) and driven by the endogenous *AGP21* promoter in
217 *agp21* (*AGP21p::V-AGP21*^{ALA}*/agp21*). Mass spectrometry had detected that all three proline
218 units (Pro/P) within the AGP21 sequence ATVEAPAPSPTS can be hydroxylated as
219 ATVEAOAOSOTS (Hyp= O) (Schultz et al. 2004), indicating likely sites for *O*-glycosylation. Even
220 though AGP21^{ALA} protein was detected in root epidermal cells (**Figure S2B**), AGP21^{ALA} failed to
221 rescue the *agp21* RH phenotype (**Figure 2B–C**), confirming that Hyp-linked *O*-glycans in AGP21
222 are required for its function in RH cell fate. Moreover, β-Glc-Y treatment did not induce anoma-
223 lous RH cell fate in AGP21^{ALA} plants demonstrating that β-Glc-Y requires *O*-glycans to alter RH
224 development.
225
226 To localize AGP21 within cells, we transiently expressed *V-AGP21* in *Nicotiana benthamiana* and
227 induced plasmolysis in epidermal cells with sorbitol (80 mM). Although some signal remained
228 within cells, most V-AGP21 signal was secreted to the apoplast (i.e., between the cell wall and
229 the PM) (**Figure 2C**). When transiently expressed at high levels, AGPs with GPI-AS typically follow
230 this pattern (Zavaliev et al. 2016). Under its endogenous promoter, most AGP21 signal localized
231 to the cell surface (**Figure S2A**). V-AGP21^{ALA}, however, never reached the cell surface; retention
232 in the secretory pathway could indicate that *O*-glycans direct AGP to the PM–cell surface (**Fig-**
233 **ure S2A–B**). These data corroborate previous reports of a requirement for *O*-glycans in the se-
234 cretion and targeting of AGPs and related fasciclin-like AGPs (Xu et al 2008; Xue et al 2017).
235
236 We tested the hypothesis that AGP21 is processed and modified during its synthesis along the
237 secretory pathway. Using immunoblot analysis, we examined the apparent molecular weight of
238 AGP21 peptide in transient AGP21-overexpressing plants and in *AGP21p::V-AGP21* plants (**Fig-**
239 **ure 2D**). In the overexpressing plants, most AGP21 peptide was detected as a strong broad band
240 around ≈100–120 kDa with minor bands at ≈80 and ≈55 kDa, whereas endogenously driven
241 AGP21 produced a stronger band at ≈80 kDa and lacked the band at ≈55 kDa, suggesting that, in
242 both cases, AGP21 peptide was present in a tri-*O*-glycosylated form. Mature peptide with no
243 posttranslational modifications is approximately 30 kDa; the extra bands could be intermediate
244 single- and di-*O*-glycosylated forms of AGP21 peptide. An apparent molecular shift of ≈25–

245 30 kDa for each putative *O*-glycosylation site in AGP21 accords with AGP14 peptide, whose pro-
246 tein sequence is highly similar (Ogawa-Ohnishi & Matsubayashi 2015), and with the electropho-
247 retic migration of an AGP-xylogen molecule that contains two arabinogalactan-*O*-Hyp sites (Mo-
248 tose et al. 2004). V-AGP21^{ALA}, which lacks *O*-glycans, is not targeted to the cell surface, formed
249 puncta structures (**Figure S2B**) and showed one band close to ~55 kDa suggesting the presence a
250 dimer (**Figure 2D**). The band close to ~30 kDa might indicate the monomer. The lack of *O*-glycans
251 V-AGP21^{ALA}'s may cause to interact with itself and this is compatible with the punctuated struc-
252 ture visualized in the root epidermal cells (**Figure S2B**). A detailed analysis is required to charac-
253 terize *O*-glycosylation in AGP21.
254
255 **_O_-glycans stabilize AGP21 peptide's functional conformation**
256 To address the effect of *O*-glycan on the conformation and stability of AGP21 peptide, we
257 modeled a minimal, 15-sugar Hyp-*O*-linked arabinogalactan (AG) structure
258 ([ATVEAP(O)AP(O)SP(O)TS], **Supplementary Item 5A–B**). This is the simplest carbohydrate
259 structure characterized for a single AGP synthetic peptide (Tan et al. 2004), although complex,
260 150 residues structures exist for several AGPs (Kitazawa et al.2013). To assess the conformation
261 of AGP21 peptide and the effect of *O*-glycosylation, molecular dynamics (MD) simulations
262 considered three nonglycosylated peptides (with alanines [nG-Ala], prolines [nG-Pro], or
263 hydroxyprolines residues [nG-Hyp], respectively) and one *O*-glycosylated peptide with three
264 Hyp-*O*-glycans (**Supplementary Item 5C**). In the MD simulations, the root mean square deviation
265 (RMSD) varied up to ≈6 Å (**Supplementary Item 5D**), indicating that peptide structure may have
266 deviated from the starting type-II polyproline helix. By contrast, larger conformational
267 stabilization effects were observed in the *O*-glycosylated peptide (**Supplementary Item 5E**).
268 Individual residue RMSF analysis indicated that the peptide's stiffer region depended on the MD
269 conditions applied (**Supplementary Item 5F**). To characterize conformational profiles, we
270 measured the angle formed by four consecutive alpha carbon atoms (ζ angle) (**Table S3**). The
271 ζ angle of a type-II polyproline helix is –110 ± 15°. In this context, the *O*-glycosylated AOAOSOTS
272 peptide structure is slightly extended between Pro2–Thr7, as observed by ζ angles 2–4 closer to
273 180° (**Table S3**). Our analysis suggests that *O*-linked glycans affect the conformation and stability
274 of AGP21 peptide. This conformational change could explain, at least in part, the failure of
275 AGP21^{ALA} to complement *agp21*. How this conformational change in mature AGP21 peptide
276 without *O*-glycans affects its function in RH cell determination remains unclear.
277
278 **AGP21 acts in a BRI1–BIN2-dependent pathway to define RH cell fate**
279 We hypothesized that disrupting AGPs activity with β-Glc-Y, a mutation (i.e., *agp21*), or abnor-
280 mal glycosylation, would interfere with BR perception and *GL2* expression. We treated the triple
281 mutant *gsk* (*gsk triple*: *bin2-3 bil1 bil2*; BIL1, BIN2-like 1 and BIL2, BIN2-like 2), which almost
282 completely lacks RH cells [1], with 5 µM β-Glc-Y treatment. *Gsk triple* exhibited few contiguous
283 RH cells (**Figure 3**), suggesting that β-Glc-Y requires BIN2-BIL1-BIL2 to alter cell fate. Interest-
284 ingly, β-Glc-Y induced ≈60% contiguous RHs (**Figure 3**) in the constitutively active mutant *bin2-1*
285 (Li & Nam 2002). Furthermore, β-Glc-Y induced ≈60% contiguous RHs in *bri1-116* (which lacks BR

286 signaling and has high BIN2 activity) and little response in *bri1-301* (a weak BRI1 mutant that
287 retains some BR signaling and partial BIN2 repression). These data suggest that BR interferes
288 with AGP-mediated RH cell fate reprogramming (**Figure 3A**), confirm that active BIN2, BIL1, and
289 BIL2 are required for this reprogramming, and indicates the existence of a BR-independent re-
290 sponse related AGPs perturbation with GSK3 proteins that induces RH cell fate.
291
292 As *BRI1* expression is similar in trichoblasts and atrichoblasts (Fridman et al., 2014), we sought to
293 determine whether BRI1 acts differently in these cell types during RH cell fate determination
294 (**Figures 3B**). We examined the effect of cell type-specific *BRI1* expression on the percentage of
295 contiguous RHs in three plant lines, all in the *bri1-116* background: trichoblast-only
296 (*COBL9p::BRI1/bri1-116*), atrichoblast-only (*GL2p::BRI1-GFP/bri1-116*), and expression in both
297 cell types (*GL2p::BRI1* + *COBL9p::BRI1/bri1-116*) (Hacham et al., 2011; Fridman et al., 2014). BRI1
298 expression in atrichoblasts only did not rescue *bri1-116* (plants showed abundant contiguous
299 RHs), lines that expressed BRI1 in trichoblasts or in both cell types were similar to wild type (**Fig-**
300 **ure 3B**). Additionally, only *COBL9p::BRI1/bri1-116* was completely insensitive to β-Glc-Y while
301 the other two lines exhibited more contiguous RHs. These data imply that only the BR pathway
302 in atrichoblasts is linked to AGP disruption and ectopic RH development.
303
304 **Disturbance or absence of AGP21 blocks *GL2* expression**
305 We tracked epidermal cell fate and analyzed β-Glc-Y and α-Man-Y's translational effects on
306 several markers: an early RH marker (RHD6p::RHD6-GFP), a downstream transcription factor
307 (RSL4p::RSL4-GFP), a late RH marker (EXP7p::EXP7-GFP), and an atrichoblast marker GL2
308 (GL2p::GL2-GFP) (**Figure 4A–D**). β-Glc-Y, not α-Man-Y, repressed GL2 expression and enhanced
309 RHD6, RSL4 and EXP7 expression in contiguous epidermal cells (**Figure 4A–E**). This corroborates
310 the effects of both β-Glc-Y and deficiencies in the AGP *O*-glycosylation pathway on contiguous
311 epidermis cell development. When we expressed RSL4p::RSL4-GFP in *agp21*, two contiguous
312 epidermis cells showed GFP expression, while this rarely occurred in wild type roots;
313 GL2p::GFP/*agp21* showed discontinuous RH patterning similar to β-Glc-Y treatment (**Figure 4B**
314 and **4D**). This result implies feedback between aberrant AGP21, GL2 repression, and RHD6-RSL4
315 and EXP7 upregulation in contiguous epidermal cell development (**Figure 4E**). Constitutively
316 active *bin2-1* phenocopies *agp21* and β-Glc-Y treatment: it represses GL2 expression in some
317 epidermal cells and enhances EXP7-GFP in contiguous epidermal cells, stimulating contiguous RH
318 development (**Figure 4F–G**). This suggests that AGP21 acts on GL2 in BIN2-dependent manner
319 and affects BR perception at the cell surface.
320
321 **AGP21 influences cell surface BR perception, modifying RH cell fate**
322 To test whether AGP21 (and AGPs in general), affect BR perception, we treated roots with
323 100 nM BL. Wild type roots exhibited repressed RH development as previously reported [1];
324 *agp21* and three glycosyltransferase mutants (*triple hpgt, ray1* and *galt29A*) defective in AGP *O*-
325 glycosylation were unaffected (**Figure S2C**), suggesting that *O*-glycosylated AGP21 promotes BR
326 perception and signaling. We hypothesized that AGP21 would closely associate with BRI1–BAK1

327 receptors, possibly affecting BR perception and BIN2 signaling to influence RH cell fate. BRI1–
328 BAK1 proteins form hetero-oligomers in specific microdomains at the PM (Wang et al. 2015)
329 where the environment restricts lateral diffusion (Hutten et al. 2017). We examined whether
330 AGP21 expressed in *Nicotiana benthamiana* colocalized with the BRI1 coreceptor BAK1
331 (**Figure S3A–B**). V-AGP21 partially colocalized with BAK1-mRFP protein, suggesting they exist in
332 close to the PM (**Figure S3A**). When epidermal cells were plasmolyzed, most AGP21 signal
333 localized to the apoplast but some remained close to the PM (**Figure S3B**), implying that AGP21
334 lies close to BAK1 and influences BR perception and BIN2-mediated RH cell fate programming in
335 atrichoblasts. Immunoprecipitation failed to detect an interaction between V-AGP21 and BAK1-
336 mRFP in a transient expression system (results not shown). Nonetheless, measuring direct
337 physical interactions between *O*-glycosylated AGP21 and BRI1–BAK1 in the apoplast–PM space
338 could support a direct interaction and would corroborate for the first time a role for an AGP
339 peptide in BR perception on the plant cell surface.
340
341 **Conclusions**
342 In root epidermal cells, atrichoblast fate is the default, while environmental as well as endoge-
343 nous cues like high levels of BRs promotes *GL2* expression in atrichoblasts to repress RH devel-
344 opment (Cheng et al. 2014). In the absence of BRs, active P-BIN2 represses *GL2* expression and
345 *RHD6* and *RSL4* expression proceeds, triggering RH development in atrichoblasts and producing
346 contiguous RHs. Abnormal AGPs at the cell surface stimulate ectopic RH development similar to
347 that observed in BR mutants. BZR1 regulates *AGP21* expression and the *O*-glycosylated cell sur-
348 face peptide AGP21 modulates RH cell fate. We propose a model, in which the *O*-glycosylated
349 AGP21 peptide is transiently linked to the PM by de GPI anchor and localizes close to BAK1 (and
350 potentially also BRI1), and thereby influences BR perception and BIN2 (and BIL1-BIL2)-mediated
351 responses, controlling root epidermal cell fate (**Figure S4**). In concordance with this scenario,
352 other GPI anchor proteins (e.g. like LORELEI-like-GPI-anchored protein 2 and 3, LRE/LLG2,3) are
353 able to interact with CrRLK1s (e.g. FERONIA and BUP1,2/ANXUR1,2) in the cell surface of polar
354 growing plant cells (Li et al. 2015; 2016; Lui et al. 2016; Ge et al. 2019; Feng et al.2019). In addi-
355 tion, a BR-independent response links AGP21 peptide (and AGPs) to a downstream BIN2 compo-
356 nent that also promotes RH cell development via an unknown molecular connection. These re-
357 sults imply an interesting parallel between plant AGPs and animal heparin sulfate proteoglycans
358 (HSPGs), which are important coreceptors in signaling pathways mediated by growth factors,
359 including members of Wnt/Wingless, Hedgehog, transforming growth factor-β, and fibroblast
360 growth factor family members (Lin 2004). The molecular mechanisms by which *O*-glycosylated
361 AGP21 peptide affects BR perception by BRI1–BAK1 remain unclear. Future work should investi-
362 gate the roles of AGP21 peptide and *O*-glycans in BR perception by root epidermal cells.

Acknowledgements

We thank ABRC (Ohio State University) for providing T-DNA lines seed lines. We would like to thank Dr. Sigal Savaldi-Goldstein for providing Gl2p::BRI1-GFP, COBL9p::BRI1-GFP and Gl2p::BRI1-GFP + COBL9p::BRI1-GFP reporter lines, Dr. Paul Dupree for providing *fut4* and *fut6* mutant lines, Dr. Santiago Mora García for providing *bzr1* and *bes1* mutant lines, Dr. Ana Caño Delgado for providing seeds of BRI1-GFP, *bin2-1* and BZR-YFP, and Dr. Gustavo Gudesblat for providing *gsk triple* mutant seeds. Dr. Malcolm Bennet and Dr. Liam Dolan for the RHD6-GFP and RSL4-GFP lines. This work was supported by grants from ANPCyT (PICT2014-0504, PICT2016-0132 and PICT2017-0066) and ICGEB CRP/ARG16-03 to J.M.E.

Author Contribution

C.B, J.G.D and M.M.R performed most of the experiments, analysed the data and wrote the paper. L.P.F and H.V. performed molecular dynamics simulations and analysed this data. M.C.S analysed the phenotype of glycosyltransferase mutants and BRI1-GFP reporters. B.V. analysed the molecular dynamics simulations data. M.C synthesized the α-Man-Y and the β-Glc-Y reagents. G.S. commented on the project, read the manuscript, and commented on the results. S.M. and E.M. analysed the data and commented on the results. J.M.P., D.R.R.M., Y.R., and S.M.V commented on the results. J.M.E. designed research, supervised the project, and wrote the paper. This manuscript has not been published and is not under consideration for publication elsewhere. All the authors have read the manuscript and have approved this submission.

383 **References**

384 Balcerowicz, D., Schoenaers, S. and Vissenberg, K. (2015). Cell fate determination and the switch
385 from diffuse growth to planar polarity in Arabidopsis root epidermal cells. *Front. Plant Sci.* 6,
386 949

387 Barnett, N.M. (1970) Dipyridyl-induced Cell Elongation and Inhibition of Cell Wall Hydroxyproline
388 Biosynthesis. *Plant Physiol* 45: 188-191

389 Cheng, Y., Zhu, W., Chen, Y., Ito, S., Asami, T. and Wang, X. (2014). Brassinosteroids control root
390 epidermal cell fate via direct regulation of a MYBbHLH-WD40 complex by GSK3-like kinases.
391 *eLife* 3, e02525

392 Ding L. and Zhu JK. (1997). A role for arabinogalactan-proteins in root epidermal cell expansion.
393 *Planta* 203:289–94

394 Feng H., Liu C., Fu R., Zhang M., Li H., Shen L., Wei Q., Sun X., Xu L., Ni B., and Li C. (2019).
395 LORELEI-LIKE GPI-ANCHORED PROTEINS 2/3 regulate pollen tube growth as chaperones and
396 coreceptors for ANXUR/BUPS receptor kinases in *Arabidopsis*. Mol. Plant.
397 doi.org/10.1016/j.molp.2019.09.004.

398 Ge Z., Zhao Y., Liu M-Ch, Zhou L-Z, Wang, L., Zhong S., Hou, S., Jiang, J., Liu, T., Huang, Q., Xiao, J.,
399 Gu, H., Wu H-M, Dong J., Dresselhaus T., Cheung A.Y., Qu L-J. (2019) LLG2/3 are co-receptors
400 in BUPS/ANX-RALF signaling to regulate Arabidopsis pollen tube Integrity. Current Biology 29,
401 1–10.

402 Guan Y, Nothnagel EA (2004) Binding of arabinogalactan proteins by Yariv phenylglycoside trig-
403 gers wound-like responses in *Arabidopsis* cell cultures. Plant Physiol 135:1346–136

404 Hacham Y, Holland N, Butterfield C, Ubeda-Tomas S, Bennett MJ, Chory J, Savaldi-Goldstein S.
405 (2011). Brassinosteroid perception in the epidermis controls root meristem size. *Development*
406 *(Cambridge, England)* 138:839–848. doi: 10.1242/dev.061804.

407 Hothorn M, Belkhadir Y, Dreux M, Dabi T, Noel JP, Wilson IA, Chory J. (2011). Structural basis of
408 steroid hormone perception by the receptor kinase BRI1. *Nature* 474:467–471. doi:
409 10.1038/nature10153.

410 Hutten SJ, Hamers DS, Aan den Toorn M, van Esse W, Nolles A, BuÈcherl CA, et al. (2017) Visuali-
411 zation of BRI1 and SERK3/BAK1 nanoclusters in *Arabidopsis* roots. *PLoS ONE* 12(1):
412 e0169905.doi:10.1371/journal.pone.01699056

413 Kitazawa K, Tryfona T, Yoshimi Y, et al. (2013). β-Galactosyl Yariv Reagent Binds to the β-1,3-
414 Galactan of Arabinogalactan Proteins. *Plant Physiology* 161(3): 1117-1126.
415 doi:10.1104/pp.112.211722.

416 Kuppusamy KT, Chen AY, Nemhauser JL. (2009). Steroids are required for epidermal cell fate es-
417 tablishment in Arabidopsis roots. Proceedings of the National Academy of Sciences of the
418 United States of America 106: 8073–8076. doi: 10.1073/pnas.0811633106.

419 Li J, Chory J. (1997). A putative leucine-rich repeat receptor kinase involved in brassinosteroid
420 signal transduction. *Cell* 90:929–938. doi: 10.1016/S0092-8674(00)80357-8

421 Li J, Nam KH (2002) Regulation of brassinosteroid signaling by a GSK3/SHAGGY-like kinase. *Sci-*
422 *ence* 295(5558):1299–1301

423 Li, C., Wu, H.-M., and Cheung, A.Y. (2016). FERONIA and her pals: functions and mechanisms.
424 Plant Physiol. 171, 2379–2392.

425 Li, C., Yeh, F.L., Cheung, A.Y., Duan, Q., Kita, D., Liu, M.C., Maman, J., Luu, E.J., Wu, B.W., Gates,
426 L., et al. (2015). Glycosylphosphatidylinositol anchored proteins as chaperones and co-
427 receptors for FERONIA receptor kinase signaling in Arabidopsis. eLife 4, e06587

428 Liang,Y., Basu,D., Pattathil,S., Xu, W.-L., Venetos, A., Martin, S.L.,et al. (2013). Biochemical and
429 physiological characterization of fut4 and fut6 mutants defective in arabinogalactan-protein
430 fucosylation in *Arabidopsis*. *J. Exp. Bot.* 64, 5537–5551. doi:10.1093/jxb/ert321
431 Lin X. (2004). Functions of heparan sulfate proteoglycans in cell signaling during development.
432 *Development* 131 (24): 6009-6021.
433 Lin, Q., Ohashi,Y., Kato,M., Tsuge,T., Gu,H., Qu,L.J., and Aoyama, T. (2015). GLABRA2 directly
434 suppresses basic helix-loop-helix transcription factor genes with diverse functions in root hair
435 development. *Plant Cell* 27: 2894–2906
436 Liu, X., Castro, C., Wang, Y., Noble, J., Ponvert, N., Bundy, M., Hoel, C., Shpak, E., and Palanivelu,
437 R. (2016). The role of LORELEI in pollen tube reception at the interface of the synergid cell and
438 pollen tube requires the modified eight-cysteine motif and the receptor-like kinase FERONIA.
439 Plant Cell 28, 1035–1052.
440 Ma Y, Zeng W, Bacic A, Johnson K (2018). AGPs trough time and space. *Annual Plant Reviews* 1,
441 1-38.
442 Majamaa K, Gunzler V, Hanauske-Abel HM, Myllyla R, Kivirikko KI (1986) Partial identity of the 2-
443 oxoglutarate and ascorbate binding sites of prolyl 4-hydroxylase. *J Biol Chem* 261: 7819-7823
444 Masucci JD, Schiefelbein JW. (1994). The *rhd6* mutation of *Arabidopsis thaliana* alters root-hair
445 initiation through an auxin- and ethylene-associated process. *Plant Physiology* 106:1335–
446 1346. doi: 10.1104/pp.106.4.1335.
447 Masucci JD, Schiefelbein JW. (1996). Hormones act downstream of *TTG* and *GL2* to promote root
448 hair outgrowth during epidermis development in the Arabidopsis root. *The Plant Cell* 8:1505–
449 1517. doi: 10.1105/tpc.8.9.1505.
450 Motose, H. et al. (2004) A proteoglycan mediates inductive interaction during plant vascular de-
451 velopment. *Nature* 429, 873–878
452 Ogawa-Ohnishi, M., Matsubayashi, Y. (2015). Identification of three potent hydroxyproline O-
453 galactosyltransferases in *Arabidopsis*. *Plant J.* 81, 736–746. doi: 10.1111/tpj.12764
454 Pereira, A.M., Pereira, L.G., and Coimbra, S. (2015). Arabinogalactan proteins: rising attention
455 from plant biologists. *Plant Reprod.* 28, 1–15.
456 Ryu KH, Kang YH, Park YH, Hwang I, Schiefelbein J, Lee MM. (2005). The WEREWOLF MYB protein
457 directly regulates *CAPRICE* transcription during cell fate specification in the *Arabidopsis* root
458 epidermis. *Development (Cambridge, England)* 132:4765–4775. doi: 10.1242/dev.02055.
459 Sardar HS, Yang J, Showalter AM (2006) Molecular interactions of arabinogalactan proteins with
460 cortical microtubules and F-actin in Bright Yellow-2 tobacco cultured cells. *Plant Physiol* 142:
461 1469–1479
462 Savaldi-Goldstein S, Peto C, Chory J. (2007). The epidermis both drives and restricts plant shoot
463 growth. *Nature* 446:199–202. doi: 10.1038/nature05618
464 Schiefelbein, J., Huang, L. and Zheng, X. (2014). Regulation of epidermal cell fate in Arabidopsis
465 roots: the importance of multiple feedback loops. *Front. Plant Sci.* 5, 47
466 Schultz CJ, Ferguson KL, Lahnstein J, Bacic A (2004) Post-translational modifications of
467 arabinogalactan-peptides of Arabidopsis thaliana: endoplasmic reticulum and
468 glycosylphosphatidylinositol-anchor signal cleavage sites and hydroxylation of proline. *J Biol*
469 *Chem* 279: 45503–45511
470 Seifert, G.J. and Roberts, K. (2007). The biology of arabinogalactan proteins. *Annual Review of*
471 *Plant Biology* **58**: 137–161
472 She J, Han Z, Kim TW, Wang J, Cheng W, Chang J, Shi S, Wang J, Yang M, Wang ZY, Chai J. (2011).
473 Structural insight into brassinosteroid perception by BRI1. *Nature* 474:472–476. doi:
474 10.1038/nature10178

475 Song SK, Ryu KH, Kang YH, Song JH, Cho YH, Yoo SD, Schiefelbein J, Lee MM. (2011). Cell fate in
476 the Arabidopsis root epidermis is determined by competition between WEREWOLF and CA-
477 PRICE. *Plant Physiology* 157:1196– 1208. doi: 10.1104/pp.111.185785.
478 Sun, Y., Fan, X.Y., Cao, D.M., Tang, W., He, K., Zhu, J.Y., He, J.X., Bai, M.Y., Zhu, S., Oh, E., et al.
479 (2010). Integration of brassinosteroid signal transduction with the transcription network for
480 plant growth regulation in Arabidopsis. *Dev. Cell* 19, 765–777
481 Tan, L., Showalter, A.M., Egelund, J., Hernandez-Sanchez, A., Doblin M.S., and Bacic, A. (2012).
482 Arabinogalactan-proteins and the research challenges for these enigmatic plant cell surface
483 proteoglycans. *Front. Plant Sci.* 3: 140
484 Tan, L., Qiu, F., Lamport, D.T.A., and Kieliszewski, M.J. (2004). Structure of a hydroxyproline
485 (Hyp)-arabinogalactan polysaccharide from repetitive Ala-Hyp expressed in transgenic
486 Nicotiana tabacum. *J. Biol. Chem.* 279: 13156–13165
487 Tryfona, T., Theys, T.E., Wagner,T., Stott,K., Keegstra, K., Dupree, P. (2014). Characterisation of
488 FUT4 and FUT6 α-(1→2)-fucosyltransferases reveals that absence of root arabinogalactan
489 fucosylation increases *Arabidopsis* root growth salt sensitivity. *PLoS ONE* 9:e93291.
490 doi:10.1371/journal.pone.0093291
491 Van Hengel AJ, Barber C, Roberts K. (2004). The expression patterns of arabinogalactan-protein
492 *AtAGP30* and *GLABRA2* reveal a role for abscisic acid in the early stages of root epidermal
493 patterning. *The Plant Journal: for Cell and Molecular Biology* 39:70–83. doi: 10.1111/j.1365-
494 313X.2004.02104.x.
495 Velasquez, S.M., Ricardi, M.M., Dorosz, J.G., Fernandez, P.V., Nadra, A.D., Pol-Fachin, L., Egelund,
496 J., Gille, S., Ciancia, M., Verli, H., et al. (2011). O-glycosylated cell wall extensins are essential
497 in root hair growth. *Science* 332:1401–1403.
498 Velasquez, SM, Ricardi MM, Poulsen CP, Oikawa A, Dilokpimol A, Halim A, et al. (2015a). Com-
499 plex regulation of prolyl-4-hydroxylases impacts root hair expansion. *Mol Plant.* 8:734–46.
500 Velasquez, S.M., Marzol, E., Borassi, C., Pol-Fachin, L., Ricardi, M.M., Mangano, S., et al. (2015b).
501 Low sugar is not always good: Impact of specific O-glycan defects on tip growth in *Arabidop-*
502 *sis*. *Plant Physiol.* 168, 808–813.doi: 10.1104/pp.114.255521
503 Wang L, Li H, Lv X, Chen T, Li R, Xue Y, et al. Spatiotemporal Dynamics of the BRI1 Receptor and
504 its Regulation by Membrane Microdomains in Living Arabidopsis Cells. *Mol Plant.* 2015;
505 8(9):1334-1349
506 Willats W.G. and Knox, J.P. (1996). A role for arabinogalactan-proteins in plant cell expansion:
507 evidence from studies on the interaction of β-glucosyl Yariv reagent with seedlings of *Ara-*
508 *bidopsis thaliana*. *Plant J.* 9:919–25
509 Xu, J., Tan, L., Lamport, D.T.A., Showalter, A.M., and Kieliszewski, M.J. (2008). The O-Hyp glyco-
510 sylation code in tobacco and Arabidopsis and a proposed role of Hyp-glycans in secretion.
511 *Phytochemistry* 69: 1631–1640
512 Xue H., Veit, C., Abas, L., Tryfona, T., Maresch, D., Ricardi, M.M., Estevez, J.M., Strasser R., Seifert
513 G.J. (2017). *Arabidopsis thaliana FLA4* functions as a glycan-stabilized soluble factor via its
514 carboxy proximal Fasciclin 1 domain. *Plant J.* 10.1111/tpj.13591
515 Yan Z, Zhao J, Peng P, Chihara RK, Li J. (2009). BIN2 functions redundantly with other Arabidopsis
516 GSK3-like kinases to regulate brassinosteroid signaling. *Plant Physiology* 150:710–721. doi:
517 10.1104/pp.109.138099
518 Yang CJ, Zhang C, Lu YN, Jin JQ, Wang XL. (2011). The mechanisms of brassinosteroids' action:
519 from signal transduction to plant development. *Molecular Plant* 4:588–600. doi:
520 10.1093/mp/ssr020

521 Yariv J, Lis H, Katchalski E (1967) Precipitation of arabic acid and some seed polysaccharides by
522 glycosylphenylazo dyes. *Biochem J* 105(1):1C–2C
523 Yi, K., Menand, B., Bell, E., and Dolan, L. (2010). A basic helix-loop-helix transcription factor con-
524 trols cell growth and size in root hairs. *Nat. Genet*. 42, 264–267. doi: 10.1038/ng.529
525 Zavaliev R., Dong, X., Epel B.L. (2016) Glycosylphosphatidylinositol (GPI) modification serves as a
526 primary plasmodesmal targeting signal. *Plant Physiology*. 172(2): 1061-1073

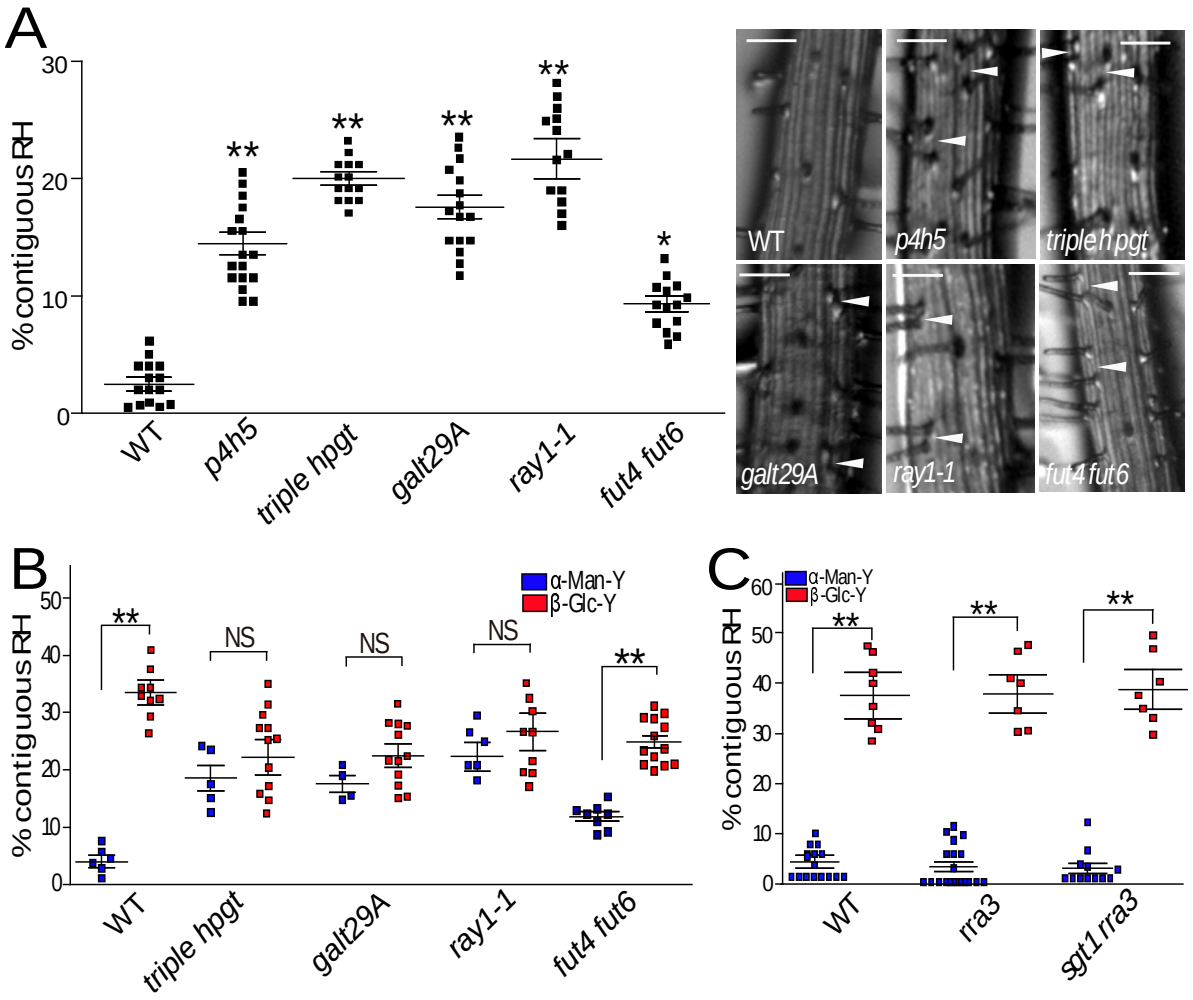

Figure 1. Contiguous RH phenotype in *O*-underglycosylated AGPs phenocopy BR mutants.

(A) RH phenotype in the *p4h5* mutant and in four glycosyltransferase mutants (*triple hpgt*, *ray1*, *galt29A*, and *fut4 fut6*) that act specifically on AGP *O*-glycosylation. Right, selected pictures. Arrowheads indicated two contiguous RHs. Scale bar= 50 µm.

(B) RH phenotype in three glycosyltransferase mutants (*triple hpgt*, *ray1*, *galt29A* and *fut4 fut6*) that act specifically on AGP *O*-glycosylation. Effect on contiguous RH phenotype in roots treated with 5µM α-Mannosyl Yariv (α-Man-Y) or 5µM β-Glucosyl Yariv (β-Glc-Y).

(C) RH phenotype in two glycosyltransferase mutants (*rra3* and *rra3 sgt1*) that act specifically on EXT *O*-glycosylation. Effect on contiguous RH phenotype in roots treated with 5µM α-Mannosyl Yariv (α-Man-Y) or β-Glucosyl Yariv (β-Glc-Y).

(A-C) *P*-value of one-way ANOVA, (**) P<0.001, (*) P<0.01. NS= not significant different. Error bars indicate ±SD from biological replicates.

See also Figure S1 and Supplementary Item 1.

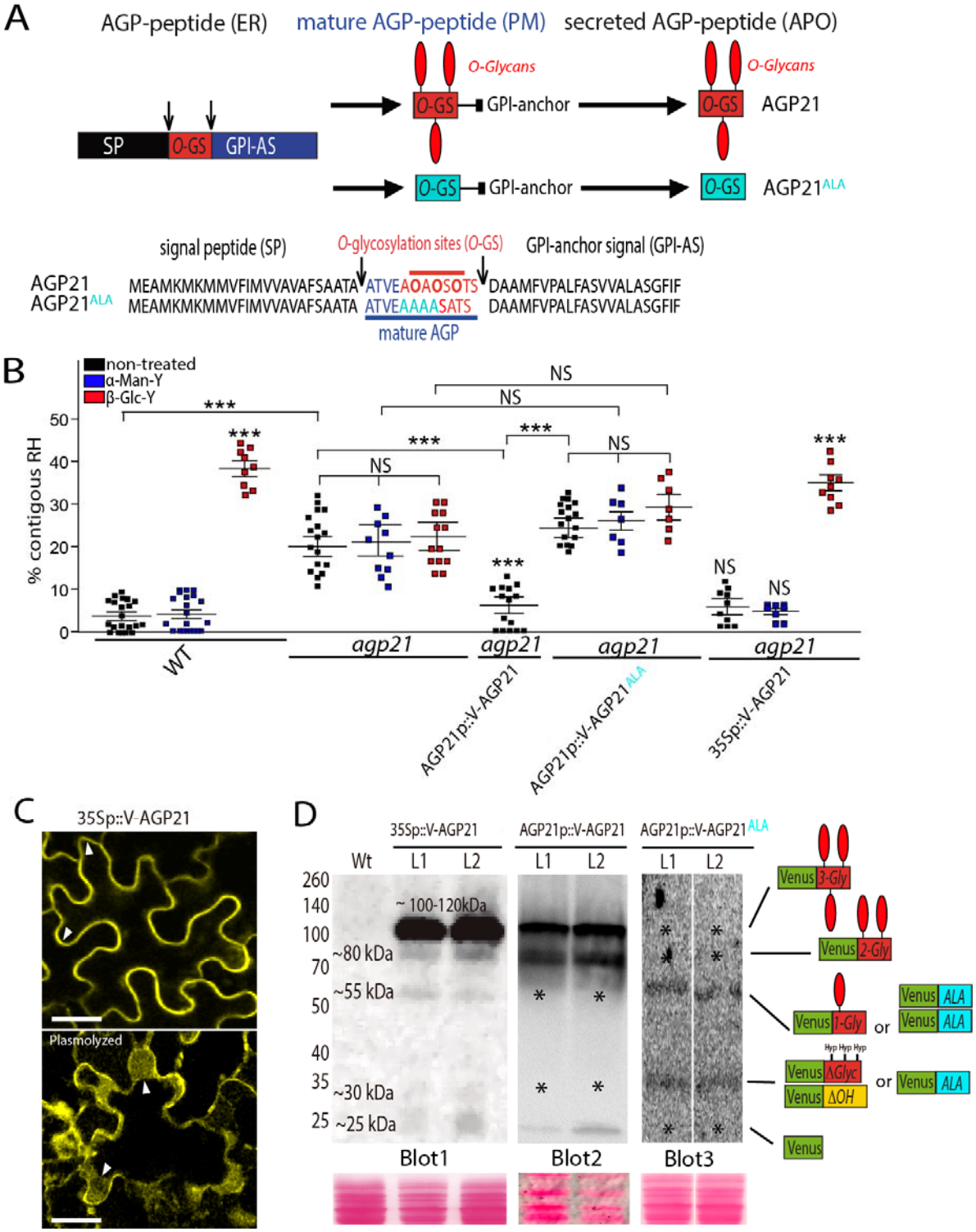

Figure 2. *O*-glycosylated AGP21 peptide at the cell surface modulates RH cell fate.

(A) Identified AGP21 peptide acting on root epidermis development. AGP21 peptide sequence and its posttranslational modifications carried out in the secretory pathway. The mature AGP21 peptide contains only 10-13 aa in length. APO= Apoplast. ER=Endoplasmic Reticulum. GPI anchor= GlycosylPhosphatidylInositol (GPI) anchor. PM=Plasma membrane.

549 (B) Contiguous RH phenotype in *agp21*, complemented *agp21* mutant with AGP21p::V-AGP21
550 and with 35Sp::V-AGP21 constructs as well as AGP21p::V-AGP21^{ALA} expression in *agp21*. Only
551 one line is shown. *P*-value of one-way ANOVA, (**) P<0.001, (*) P<0.01. NS= not significant
552 differences. Error bars indicate ±SD from biological replicates.
553 (C) Subcellular localization of 35Sp::V-AGP21 transiently expressed in *Nicotiana benthamiana* (on
554 the left) or in *Arabidopsis thaliana* (on the right). Plasmolysis (P+) induced with a Mannitol (800
555 mM) treatment (bottom pictures) showed a secretion outside the plasma membrane and in the
556 plasma membrane of AGP21 in *N. benthamiana* or only plasma membrane AGP21 localization in
557 *A. thaliana*. Arrowheads indicate plasma membrane located AGP21. Scale bar= 50 µm.
558 (D) Immunoblot analysis of two stable lines expressing 35Sp::V-AGP21 (L1-L2) and two lines
559 expressing AGP21p::V-AGP21 (L1-L2) and two lines expressing AGP21p::V-AGP21^{ALA} (L1-L2). Each
560 blot is an independent experiment. Putative Venus-AGP21 structures are indicated on the right.
561 *O*-glycans are indicated as red elongated balloons. ΔOH = non-hydroxylated. ΔGly = without *O*-
562 glycans. 1-Gly to 3-Gly = 1 to 3 sites with Hyp-*O*-glycosylation. Asterisk indicates missing AGP21
563 glycoforms or lack of Venus protein.
564 See also Figure S2 and Supplementary Items 2-5.

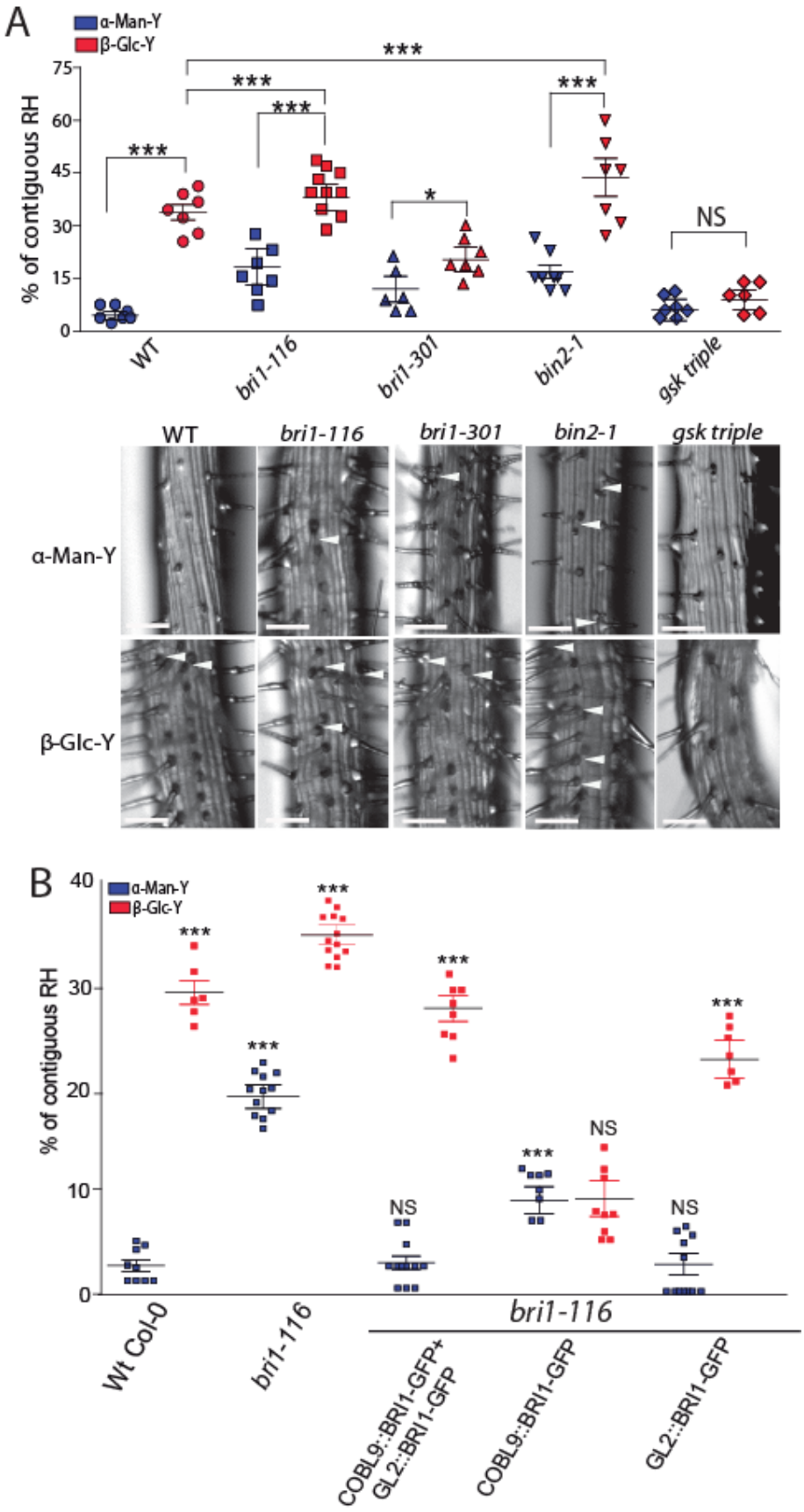
A
α-Man-Y
β-Glc-Y
% of contiguous RH
75
60
45
30
15
0
***
***
***
***
*
NS
WT
bri1-116
bri1-301
bin2-1
gsk triple
WT
bri1-116
bri1-301
bin2-1
gsk triple
α-Man-Y
β-Glc-Y
B
α-Man-Y
β-Glc-Y
% of contiguous RH
40
30
20
10
0
***
***
***
***
***
***
NS
NS
NS
Wt Col-0
bri1-116
bri1-116
COBL9::BRI1-GFP+
GL2::BRI1-GFP
COBL9::BRI1-GFP
GL2::BRI1-GFP

565

566 **Figure 3. Perturbation of AGPs requires active BRI1 expression in atrichoblast cells and**
567 **downstream BIN2-BIL1-2 proteins to triggers changes in RH cell fate**.
568 (A) Contiguous RH phenotype in roots treated with 5µM β-Glucosyl Yariv (β-Glc-Y) or 5µM α-
569 Mannosyl Yariv (α-Man-Y). Scale bar= 20 µm. *P*-value of one-way ANOVA, (***) P<0.001, (*)
570 P<0.05. NS= not significant differences. Error bars indicate ±SD from biological replicates.
571 Arrowheads indicated two contiguous RHs.
572 (B) Effect of the BRI1 differential expression on the development of contiguous RH. BRI1 is active
573 when expressed in atrichoblast cells (under GL2 promoter).
574 See also Figure S3.

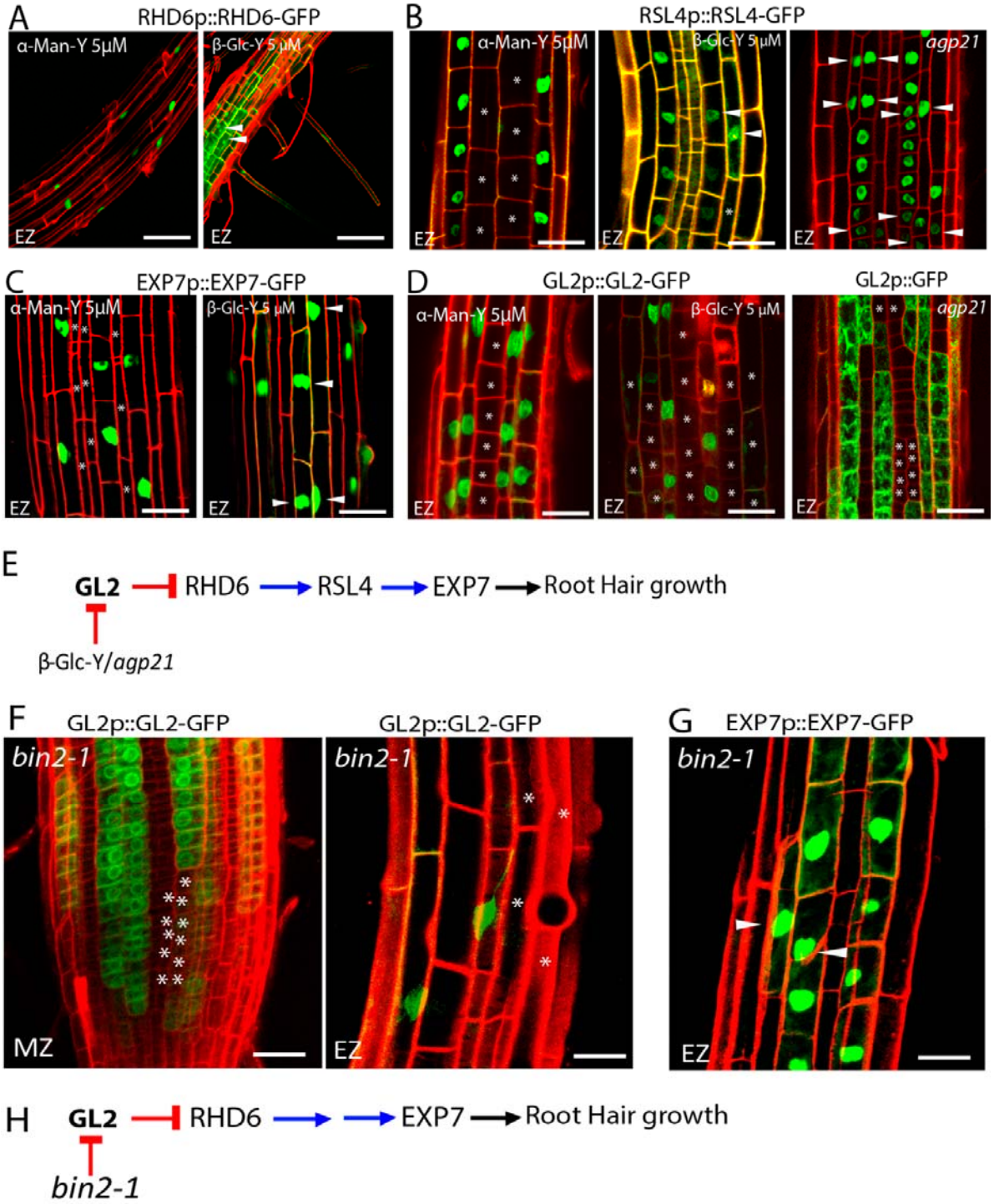

Figure 4. AGPs disruption, the lack of AGP21, and *bin2-1* block the RH repressor GLABRA2 (GL2) and triggers RHD6-RSL4-EXP7 expression in some atrichoblast cells.

The effect of β-Glucosyl Yariv (β-Glc-Y), α-Mannosyl Yariv (α-Man-Y), and the absence of AGP21 peptide were monitored on several markers to study epidermis cell fate.

(A) RHD6 (RHD6p::RHD6-GFP) as an early RH marker.

(B) A downstream RHD6 factor RSL4 (RSL4p::RSL4-GFP).

583 (C) The RSL4-gene target EXP7 (EXP7p::EXP7-GFP).
584 (D) The main RH repressor GL2 (GL2p::GL2-GFP). (A-D) Arrowheads indicate expression of a
585 given marker in two contiguous epidermis cell lines. Asterisks indicate absence of expression.
586 Scale bar= 20 µm.
587 (E) Proposed sequence of events triggered by β-Glucosyl Yariv (β-Glc-Y) or the lack of AGP21
588 peptide that leads to abnormal RH development.
589 (F) GL2 expression in the *bin2-1* background in the Meristematic Zone (MZ) and Elongation Zone
590 (EZ) of the root.
591 (G) The RH marker EXP7 expression in the *bin2-1* background in the Elongation Zone (EZ) of the
592 root. (F-G) Arrowheads indicate expression of a given marker in two contiguous epidermal cell
593 lines. Asterisks indicated absence of expression. Scale bar= 10 µm.
594 (H) Proposed sequence of events triggered by *bin2-1* that leads to abnormal RH development.
595 See also Figure S4.

Cell surface *O*-glycosylated AGP21 peptide acts on the Brassinosteroids pathway to modulate root hair cell fate

Cecilia Borassi[1,#], Javier Gloazzo Dorosz[1,#], Martiniano M. Ricardi[2,#,*], Laercio Pol Fachin[3], Mariana Carignani Sardoy[1], Eliana Marzol[1], Silvina Mangano[1], Diana Rosa Rodríguez Garcia[1], Javier Martínez Pacheco[1], Yossmayer del Carmen Rondón Guerrero[1], Silvia M. Velasquez[1,**], Bianca Villavicencio[4], Marina Ciancia[5], Georg Seifert[6], Hugo Verli[4] & José M. Estevez[1,7,†]

Supplemental Information

Supplemental Figures S1-S4
Material and Methods
Supplementary Items Tables S1-S4
Supplementary Items Figures S1-S5
Supplementary References

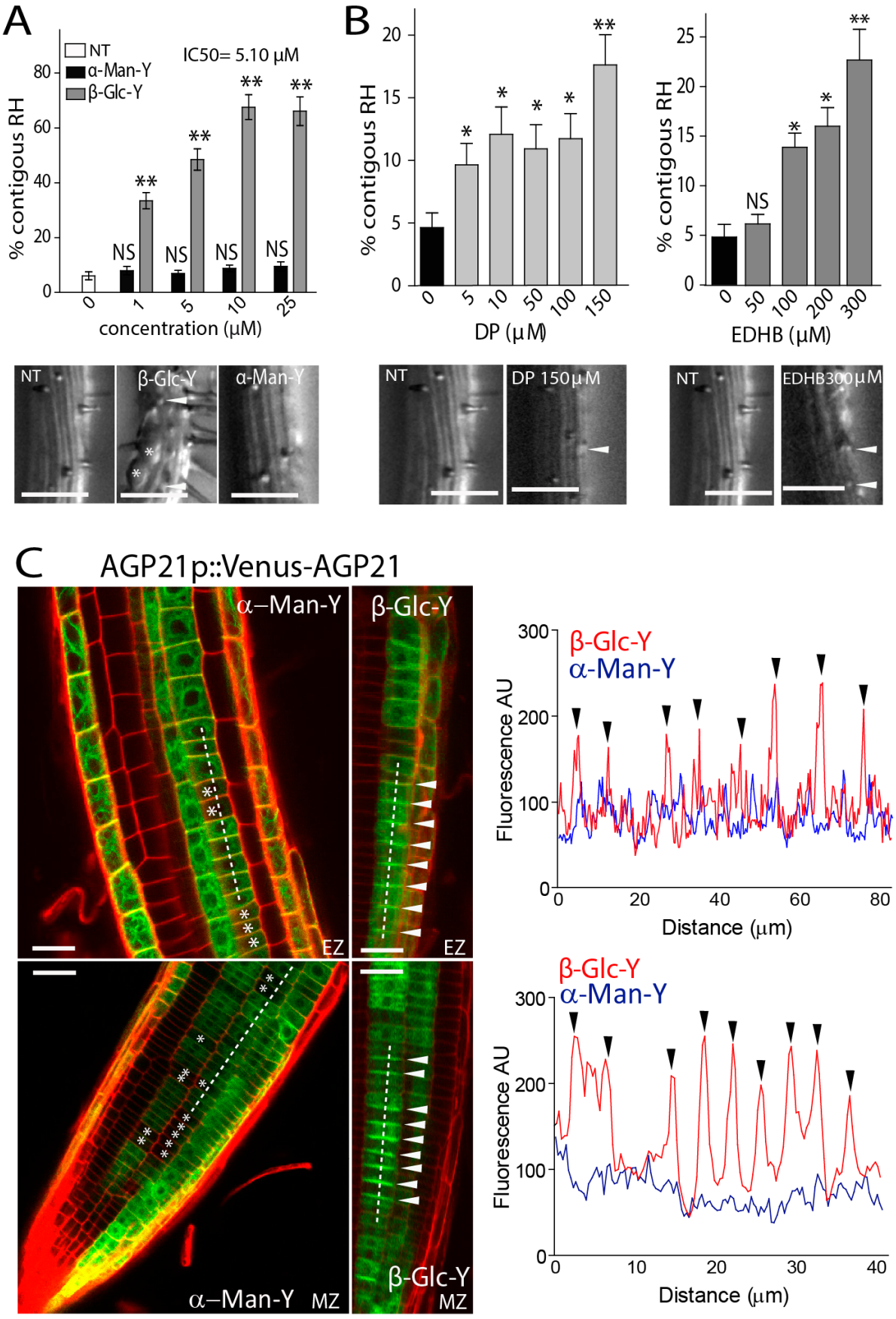
A
NT
α-Man-Y
β-Glc-Y
IC50= 5.10 µM
% contigous RH
concentration (µM)
NS
**
B
% contigous RH
DP (µM)
EDHB (µM)
NT
β-Glc-Y
α-Man-Y
DP 150µM
EDHB300µM
C
AGP21p::Venus-AGP21
α–Man-Y
β-Glc-Y
EZ
MZ
Fluorescence AU
Distance (µm)

Figure S1. Perturbation of *O*-glycosylated AGPs affect RH cell fate program. β-Glc-Y is able to trigger an over-accumulation of AGP21 peptide in the cell surface.

(A) Contiguous RH phenotype developed under pharmacological of AGPs. Pictures below each graph indicate the RH phenotype in detail. Arrowheads indicate two contiguous RH cell protuberances. Asterisk indicated bulging cells. Roots treated with β-Glucosyl Yariv (β-Glc-Y) or with α-Mannosyl Yariv (α-Man-Y) as control. NT= non-treated.

(B) Contiguous RH phenotype developed under pharmacological disruption of peptidyl-proline. Roots treated with two distinct P4H inhibitors, α,α-dipyridyl (DP) and ethyl-3,4-dihydroxybenzoate (EDHB). Pictures below each graph indicate the RH phenotype. Arrowheads indicate two contiguous RH cell protuberances. Asterisk indicated bulging cells. Scale bar= 50 µm.

(C) AGP21 is expressed in some but not all trichoblast and atrichobast cells with a discontinuous pattern (asterisk) in the meristematic zone (MZ) and elongation root zones (EZ). Some root epidermal cell layer lack AGP21 (line). On the left, the effect of β-Glucosyl Yariv (β-Glc-Y) on the accumulation of AGP21p::V-AGP21 on root epidermal cells. Arrowheads indicate cell surface AGP21 peptide over-accumulation in transversal walls in the treated roots with β-Glc-Y. Scale bars= 10 µm. Plot profiles (dashed lines) indicates the accumulation of AGP21p::V-AGP21 (black arrowheads) when roots are treated with β-Glc-Y.

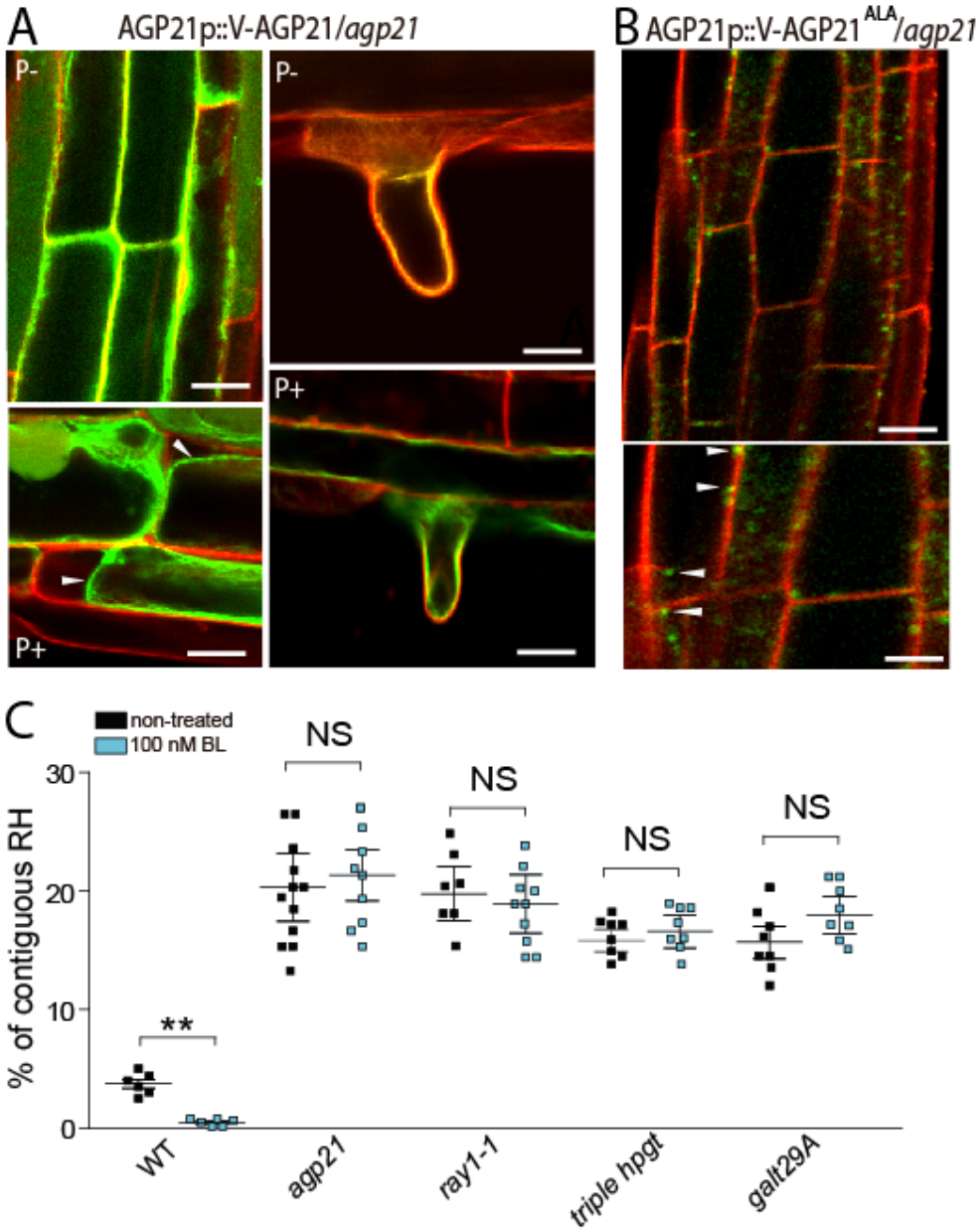

Figure S2. AGP21 expression at the cell surface in epidermis and RH cells. Perception of BR in epidermal cells is abolished in the *agp21* and related under-*O*-glycosylated AGP mutants.

(A) Expression of AGP21p::V-AGP21 at the plasma membrane in non-plasmolyzed (P-) and plasmolyzed (P+) epidermal cells (on the right) and RHs (on the left) with 800 mM Mannitol. Arrowheads indicate retraction of plasma membrane. Scale bar= 10 µm.

(B) Expression of AGP21p::V-AGP21^{ALA}. This version of AGP21 peptide accumulates as intracellular dots. Scale bar= 10 µm.

(C) Contiguous RH phenotype in WT Col-0, *agp21*, *ray1-1*, *triple hpgt* and *galt29A* in non-treated and treated roots with 100nM BL. *P*-value of one-way ANOVA, (**) P<0.001. NS= not significant different. Error bars indicate ±SD from biological replicates.

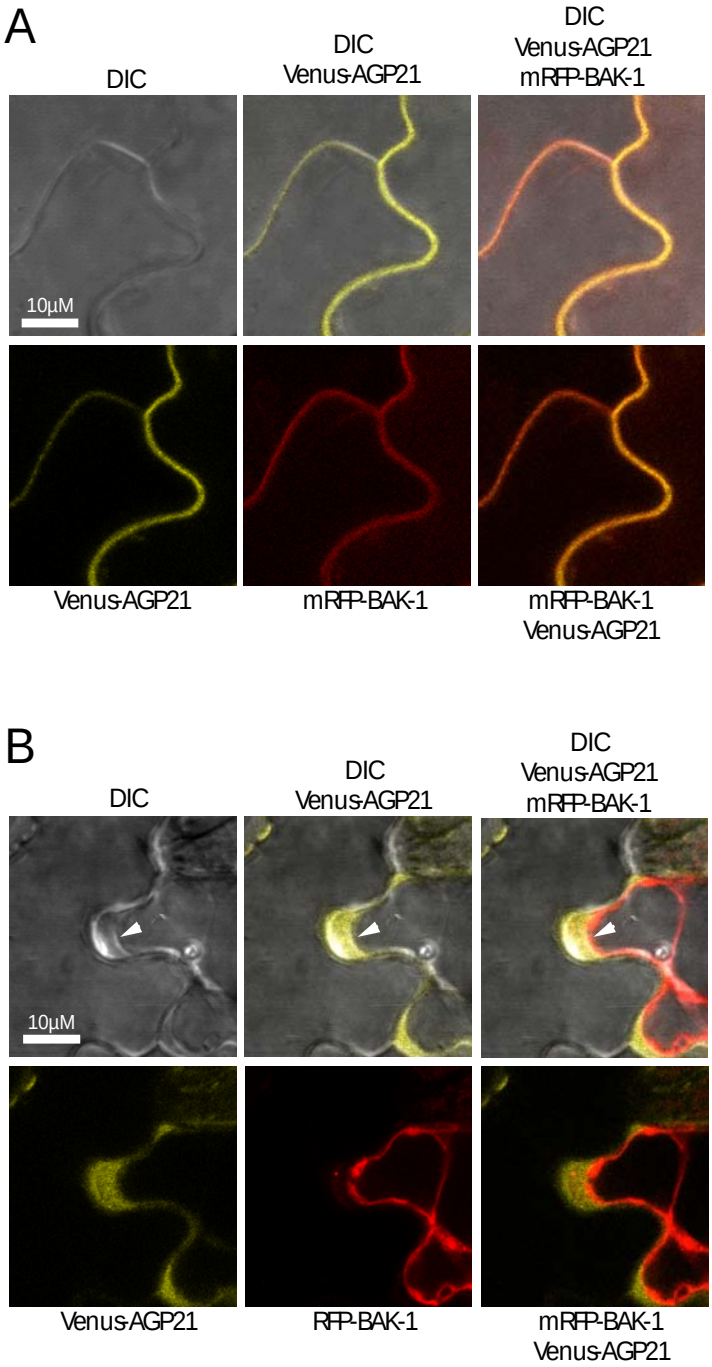

Figure S3. AGP21 partially co-localizes with BAK1 protein in epidermal cells.

(A) Co-localization of AGP21-Venus with BAK1-mRFP at the plasma membrane of epidermal cells in *Nicothiana Benthamiana*. Scale bar= 10 µm. Cross section of expression levels across BAK1-RFP coexpressed with AGP21-Venus.

(B) Plasmolysis was induced with 800 mM Mannitol uncovering an apoplastic plus plasma membrane AGP21 localization. Scale bar= 10 µm.

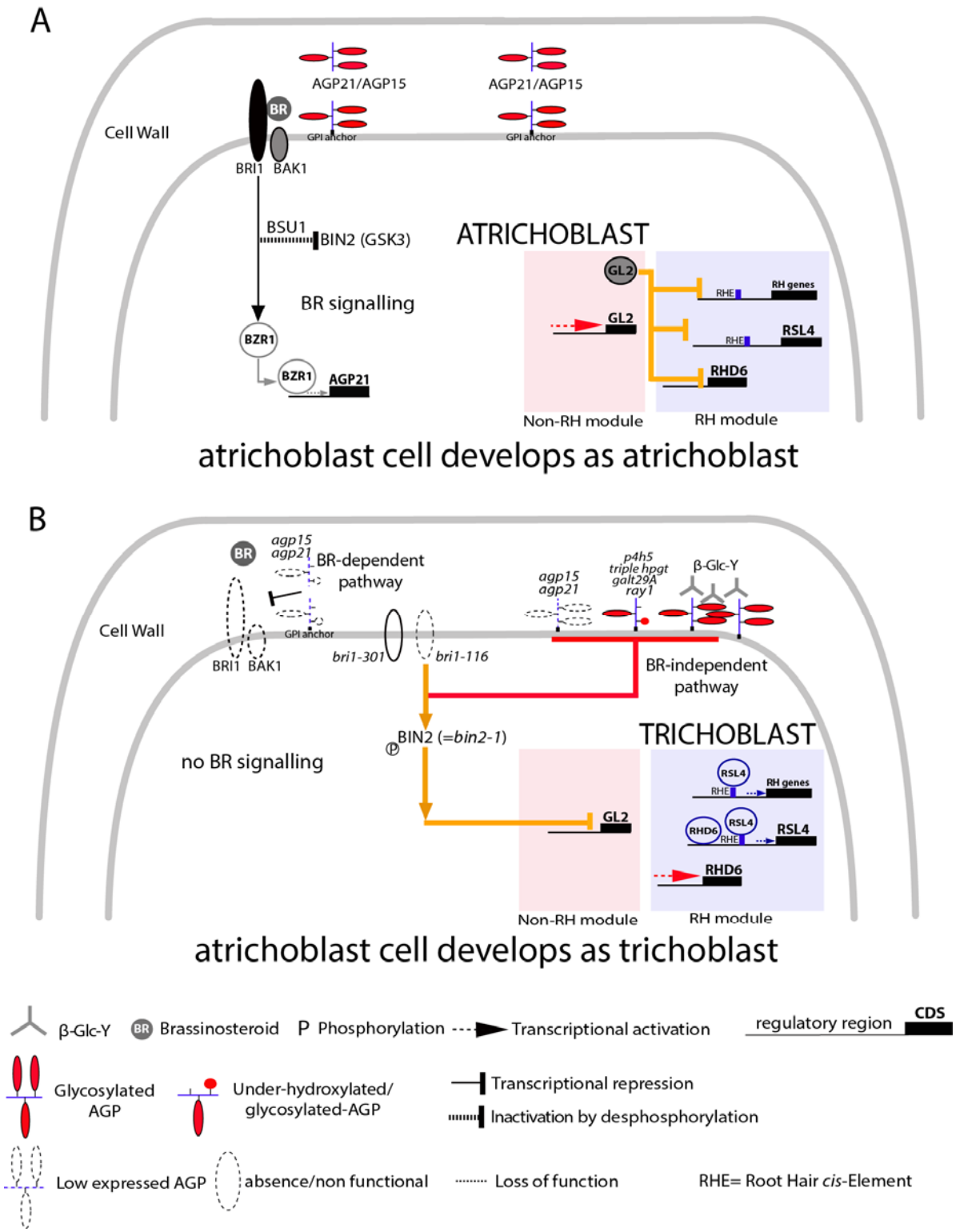

Figure S4. AGP21 influences BR perception in the root epidermis to control RH cell fate in a BIN2-dependent manner.

(A) Under normal BR-signaling. Model of BR-BRI1-BAK1 pathway modulation by plasma membrane *O*-glycosylated AGP21. BR-signalling controls RH cell fate by inhibiting

phosphorylation activity of BIN2 and impacting on GL2 expression. Most atrichoblast cells keep their cell fate identity.

(B) Disruption of *O*-glycosylated AGPs (with β-Glc-Y) and the lack of AGP21 (in *agp21* mutant) as well as abnormal glycosylated AGPs (in *p4h5, triple hpgt, ray1, galt29A* mutants and DP/EDHB treated roots) may interfere with BRI1-brassinosteroid perception and BIN2 downstream effect on the RH repressor GL2. Some atrichoblast cells lost their cell fate identity and they develop ectopic RH cells. As a consequence, GL2 transcriptional repression triggers RH development in atrichoblast cells producing contiguous RH. In this case the atricoblast cell differentiates as trichoblast. In addition, disruption of AGP21 peptide (and AGPs) act in a BR-independent manner but converges on BIN2 to triggers abnormal RH cell fate.

Materials and Methods

Growth conditions. All plant materials used in this study were in the Columbia-0 ecotype background of *Arabidopsis thaliana*. Seeds were sterilized and placed on half-strength (0.5X) Murashige and Skoog (MS) medium (Sigma-Aldrich) pH 5.8 supplemented with 0.8% agar. For root measurements, RNA extraction and confocal microscopy 7-day old seedlings were grown on square plates placed vertically at 22°C with continuous light, after stratification in dark at 4°C for 5 days on the plates. Seedlings on plates were transferred to soil and kept in the greenhouse in long-day conditions to obtain mature plants for transformation, genetic crossing, and amplification of seeds.

Plant material. For identification of homozygous T-DNA knockout lines, genomic DNA was extracted from rosette leaves. Confirmation by PCR of a unique band corresponding to T-DNA insertion in the target genes AGP15 (At5G11740: SALK_114736), AGP21 (At1G55330: SALK_140206), HPGT1-HPGT3 (AT5G53340: SALK_007547, AT4G32120: SALK_070368, AT2G25300: SALK_ 009405) GALT29A (At1G08280: SALK_030326; SALK_113255; SAIL_1259_C01) and RAY1 (At1G70630: SALK_053158) were performed using an insertion-specific LBb1.3 for SALK lines or Lb1 for SAIL lines. Primers used are listed in **Table S4**. The stable transgenic lines used in this study are summarized in **Table S2**.

Pharmacological treatments. ethyl-3,4-dihydrohydroxybenzoate (EDHB) and α,α-Bipyridyl (DP) D216305 SIGMA-ALDRICH were used as P4Hs inhibitors. DP chelates the cofactor Fe^{2+} [9] and the EDHB interacts with the oxoglutarate-binding site of P4Hs (Majamaa et al. 1986). Specific Yariv phenylglycoside (for 1,3,5-tri-(p-glycosyloxyphenylazo)-2,4,6-trihydroxybenzene), β-glucosyl Yariv phenylglycoside (β-Glc-Yariv) was used for AGP-depletion (Kitazawa et al.2013). α-mannosyl Yariv phenylglycoside (α-Man-Yariv) was used as negative control for phenylglycoside treatment. Both, β-Glc-Y and α-Man-Y are Yariv-phenylglycosides and its specificity for AGPs relies on the β-configuration of the glycosyl residues attached to the phenylazotrihydroxybenzene core (Yariv et al. 1967). DP, EDHB, or Yariv reagents were added to MS media when MS plates were made. Seedlings were grown for 4 days in MS 0.5X media and then transferred for 3 days more to MS 0.5X plates with DP, EDHB, or Yariv reagents at the concentration indicated.

Quantification of RH cell fate. In order to determine the RH patterning, images of root tips were taken using an Olympus stereomicroscope at maximum magnification (50X). The presence of contiguous RH was analyzed using ImageJ, starting from the differentiation zone to the elongation zone. The amount of contiguous RH was expressed as a percentage of total RH for rectangular root areas of 200 µm in width x 2mm in length (n=20) with three biological replicates. Quantitative and statistical analysis was carried on using GraphPad software. To analyze the alteration in RH cell fate, root cell walls of reporter lines were stained with 5 µg/ml propidium iodide and confocal microscopy images were taken using a Zeiss LSM 710 Pascal microscope, 40X objective N/A= 1.2.

112 **AGP21 variants.** AGP21 promoter region (AGP21p) comprising 1,5 Kbp upstream of +1 site was
113 amplified by PCR and cloned into pGWB4 to obtain AGP21p::GFP construct. Synthetic DNA was
114 designed containing full length AGP21 cDNA and Venus fluorescent protein cDNA between
115 AGP21 signal sequence and the mature polypeptide (Venus-AGP21), containing GatewayTM (Life
116 Technologies) attB1 and attB2 sites. Recombinase-mediated integration of the PCR fragment
117 was made into pEntry4Dual. pEntry4Dual/Venus-AGP21 construction was recombined into the
118 vector pGWB2 (Invitrogen, Hygromicyn R) in order to overexpress Venus-AGP21 under 35S
119 mosaic virus promoter (35Sp::Venus-AGP21). Also, Venus-AGP21 construct was cloned into
120 pGWB1 (no promoter, no tag) and AGP21p was sub-cloned in the resulting vector to express
121 AGP21 reporter under the control of its endogenous promoter (AGp21p::Venus-AGP21). Wild
122 type and T-DNA *agp21* mutant plants were transformed by using Agrobacterium (strain
123 GV3101+pSoup). Plants were selected with hygromycin (30 µg/ml) and several independent
124 transgenic plants were isolated for each construct. At least three homozygous independent
125 transgenic lines of Col-0/AGP21p::GFP, *agp21*/AGP21p::Venus-AGP21 and *agp21*/35Sp::AGP21-
126 GFP were obtained and characterized.
127
128 **Gene expression analysis**. For RT-PCR analysis, total RNA was isolated from roots of 7-day-old
129 seedlings using RNeasy Plant Mini Kit (Qiagen) according to the manufacturer's instructions.
130 cDNA synthesis was achieved using M-MLV reverse transcriptase (Promega). PCR reactions were
131 performed in a T-ADVANCED S96G (Biometra) using the following amplification program: 4 min
132 at 95°C, followed by 35 cycles of 20 secs at 95°C, 30 secs at 57°C and 30 secs at 72°C. RT-PCR was
133 performed to assess AGP15 and AGP21 transcript levels in wild type and T-DNA mutant *agp15*
134 and *agp21*. PP2A was used as an internal standard. All primers used are listed in **Table S4.**
135
136 **Confocal microscopy.** Confocal laser scanning microscopy was performed using Zeiss LSM 510
137 Meta and Zeiss LSM 710 Pascal. Fluorescence was analyzed by using laser lines of 488 nm for
138 GFP or 514 nm for YFP excitation, and emitted fluorescence was recorded between 490 and 525
139 nm for GFP and between 530 and 600 nm for YFP (40X objective, N/A= 1.2). Z series was done
140 with an optical slice of 2µm, and intensities was summed for quantification of fluorescence
141 along a segmented line using plot profile command in Image J, five replicates for each of five
142 roots were observed.
143
144 **AGP21 Immunoblotting detection.** Proteins were extracted from roots of 7-day-old seedlings
145 using extraction buffer (20mM TRIS-HCl pH8.8, 150mM NaCl, 1mM EDTA, 20% glycerol, 1mM
146 PMSF, 1X protease inhibitor Complete® Roche) at 4°C. After centrifugation at 21.000*g* at 4ºC for
147 20min, protein concentration in the supernatant was measured and equal protein amounts were
148 loaded onto a 6% SDS- PAGE gel. Proteins were separated by electrophoresis and transferred to
149 nitrocellulose membranes. Anti-GFP mouse IgG (Roche Applied Science) was used at a dilution of
150 1:1.000 and it was visualized by incubation with goat anti-mouse IgG secondary antibodies
151 conjugated to horseradish peroxidase (1:10.000) followed by a chemiluminescence reaction
152 (Clarity ™ Western ECL Substrate, BIO-RAD).

153
154 **Transient expression assays in *Nicotiana benthamiana*.** To test the sub-cellular localization of
155 AGP21, 5-day-old *N. benthamiana* leaves were infiltrated with *Agrobacterium* strains (GV3101)
156 carrying 35Sp::Venus-AGP21 and BAK1-RFP constructs. After 2 days, images of the lower leaf
157 epidermal cells were taken using a confocal microscope (LSM5 Pascal) to analyze Venus-AGP21
158 expression. Plasmolysis was done using 800 mM mannitol.
159
160 **Molecular dynamics (MD) simulations.** MD simulations were performed on two non-
161 glycosylated and seven glycosylated Ala1-Pro2-Ala3-Pro4-Ser5-Pro6-Thr7-Ser8 (APAPSPTS)
162 peptides, in which the starting structure was constructed as a type II polyproline helix, with ϕ ~ -
163 75 and ψ ~ 145. The non-glycosylated motifs differ by the presence of alanine (AAAASATS),
164 proline (APAPSPTS) or 4-*trans*-hydroxyproline (AOAOSOTS) residues. At the same time, the
165 glycosylated motifs reflect different peptide glycoforms, constructed as full glycosylated
166 (AOAOSOTS). Every *O*-glycosylation site was filled with an arabinogalactan oligosaccharide
167 moiety (**Supplementary Item 5**), in which the *O*-glycan chains and carbohydrate-amino acid
168 connections were constructed based on the most prevalent geometries obtained from solution
169 MD simulations of their respective disaccharides, as previously described (Pol-Fachin & Verli
170 2012), thus generating the initial coordinates for glycopeptide MD calculations. Such structures
171 were then solvated in rectangular boxes using periodic boundary conditions and the SPC water
172 model (Berendsen et al. 1984). Both carbohydrate and peptide moieties were described under
173 GROMOS96 43a1 force field parameters, and all MD simulations and analyses were performed
174 with GROMACS simulation suite, version 4.5.4 (Hess et al. 2008). The Lincs method (Hess et al.
175 1997) was applied to constrain covalent bond lengths, allowing an integration step of 2 fs after
176 an initial energy minimization using the Steepest Descents algorithm. Electrostatic interactions
177 were calculated with the generalized reaction-field method Tironi et al. (1995). Temperature and
178 pressure were kept constant at 310 K and 1.0 atom, respectively, by coupling (glyco)peptides
179 and solvent to external baths under V-rescale thermostat Bussi et al. 2007) and Berendsen
180 barostat (Berendsen et al. 1987) with coupling constants of t =0.1 and t=0.5, respectively, via
181 isotropic coordinate scaling. The systems were heated slowly from 50 to 310 K, in steps of 5 ps,
182 each one increasing the reference temperature by 50 K. After this thermalization, all simulations
183 were further extended to 100 ns. See **Table S3**.

184 **Table S1**. GTs involved in AGP modification used in this study.

185

Protein/Gene code	CAZY family	Full name/ Activity	References
Enzymes acting on AGP and related glycoproteins			
HPGT1/AT5G53340 **HPGT2/**AT4G32120 **HPGT3/**AT2G25300	GT31	Hydroxyproline Galactosyltransferases 1-3/ transfer of D-Gal*p* to the hydroxyl-group on Hyp residues in AGPs and related glycoproteins	Egelund et al. 2007
GalT29A/AT1G08280	GT29	Galactosyltransferase 29A/ transfers galactose in β-D-(1→6) position as elongating enzyme or in β-D-(1→3)-galactosyl oligosaccharides	Dilokpimol et al. 2014; Geshi et al. 2013
RAY1/AT1G70630	GT77	Reduced Arabinose Yariv 1/ β-arabinofuranosyltransferase that adds arabinose on the AGP backbone	Gille et al. 2013
FUT4/AT2G15390 **FUT6/**AT1G14080	GT77	Fucosyltransferase/ transfers fucose as α-L-(1→2) position to α-L-Ara*f*-(1→) unit	Tryfona et al 2014
Enzymes acting on EXTs and related glycoproteins			
RRA3/AT1G19360	GT77	Reduced Residual Arabinose 3/ Arabinosyltransferase that transfers of β-L-Ara*f* -(1→2) units	Egelund et al. 2007 Velasquez et al. 2011
SGT1 (SERGALT1) /At3g01720	GT96	peptidyl serine *O*-α-galactosyltransferase	Saito et al. 2014

186

187 **Table S2**. Mutants and transgenic lines generated and used in this study.

Gene name	AGI code	Genetic background	Transgenic line	Reference
RRA3	AT1G19360	*rra3*	-	Egelund et al. 2007 Velasquez et al. 2011
SGT1	At3g01720	*sgt1 (sergalt1) rra3*	-	Saito et al. 2014 Velasquez et al. 2015a
P4H5	AT2G17720	*p4h5*	-	Velasquez et al. 2011
GalT29A	AT1G08280	*galt29A*	-	Dilokpimol et al. 2014; Geshi et al. 2013
RAY1	AT1G70630	*ray1*	-	Gille et al. 2013
AGP15	AT5G11740	*agp15* *agp15,agp21*	-	This work This work
AGP21	AT1G55330	*agp21* *agp21* *agp21* Col-0 Col-0	- 35Sp::Venus-AGP21 AGP21p::Venus-AGP21 35Sp::Venus-AGP21 AGP21p::GFP	This work This work This work This work This work
Brassinosteroid lines				
BRI1	AT4G39400	*bri1-5* *bri1-116* *bri1-116*	- - AGP21p::GFP 35Sp::BRI1-GFP	Noguchi et al. 1999 Li & Chory 1999 This work
BZR1	AT1G75080	bzr1-D Col-0	BZR1p::BZR1-YFP 35Sp::BZR1-GFP BZR1-D *bzr1-1 crispr-cas*	Wang et al. 2002 Chaiwanon et al. 2015 Saito et al. 2018
BES1	AT1G19350	bes1-D	- 35Sp::BES1-GFP BES1-D *Bes1-1 bzr1-1 crispr-cas*	Yin et al. 2002 Saito et al. 2018
BIN2	AT4G18710	*bin2-1* *bin2,bil1,bil2*	BIN2p:BIN2-GFP	Yin et al. 2002
BIL1	AT2G30980		-	Kim 2012 Yan et al. 2009
BIL2	AT1G06390		-	
Trichoblast and Atrichoblast marker lines				
RHD6	AT1G66470	Wt Col-0	RHD6p::RHD6-GFP	Yi et al. 2010

RSL4	AT1G27740	Wt Col-0	RSL4p::RSL4-GFP	Yi et al. 2010
GL2	AT1G79840	Wt Col-0	GL2p::GL2-GFP	Lin et al. 2015
EXP7	AT1G12560	Wt Col-0	EXP7p::nGFP	Kim et al. 2006

188

189 **Table S3**. Average ζ angle values* during the performed MD simulations of AGP21 peptide.
190

Peptide state	ζ angle 1 Ala1-Pro2-Ala3-Pro4	ζ angle 2 Pro2-Ala3-Pro4-Ser5	ζ angle 3 Ala3-Pro4-Ser5-Pro6	ζ angle 4 Pro4-Ser5-Pro6-Thr7	ζ angle 5 Ser5-Pro6-Thr7-Ser8
Type-II polyproline	-110 ± 15	-110 ± 15	-110 ± 15	-110 ± 15	-110 ± 15
non-Glyco, Ala AGP21	**159 ± 89**	**149 ± 116**	**153 ± 126**	**166 ± 97**	**-177 ± 75**
non-Glyco, Pro AGP21	-124 ± 46	-125 ± 31	-130 ± 49	-130 ± 31	-149 ± 49
non-Glyco, Hyp AGP21	-130 ± 47	-125 ± 31	-133 ± 46	-128 ± 32	-150 ± 51
Glyco1,2,3 AGP21	**-112 ± 25**	**-175 ± 16**	**-168 ± 22**	**-150 ± 21**	**-131 ± 43**

191 * Average ± standard deviation values measured for the second half of MD simulations (from 50 ns to 100 ns).

Table S4. Primers used in this study.

Purpose	Name	Sequence (5' to 3')
RT-PCR AGP15	Forward	CATCGGCACAATCTGAGG
	Reverse	ACCATCACAGTAACTTAGATCC
RT-PCR AGP21	Forward	GCAATGAAGATGAAGATGATGG
	Reverse	TCAGAAGTTGGGCTTGGAG
RT-PCR PP2A	Forward	TCCGAGATCACATGTTCCAAACTC
	Reverse	CCGTATCATGTTCTCCACAACCG
T-DNA AGP15	Forward	GACACGAAAGACGCTGAGATC
	Reverse	AGGAGAAATTTGCACCCATTC
T-DNA AGP21	Forward	TTTGGTGTGAACGTTGGTATG
	Reverse	CAAAAGATGAAACCAGATGCC
T-DNA GALT29A	Forward	TTTGTGGCTCGAGTAAACCC
	Reverse	AAGCATGAGATTGTGATTCGG
T-DNA RAY1	Forward	TTTGGAGCGTATGGATCAAAG
	Reverse	GAGTTATGCTCACGAGCTTGG
Promoter AGP21	Forward	TAATGCCAACTTTGTACAAAAAAGCAGGCT
	Reverse	CCCAGCTTTCTTGTAC
Venus-AGP21	Forward	GGGGACAAGTTTGTACAAAAAAGCAGGCTTAACCatggaggcaatgaagatg
	Reverse	GGGGACCACTTTGTACAAGAAAGCTGGGTCtcaaaagatgaaaccaga
RT-PCR AGP15	Forward	CATCGGCACAATCTGAGG
	Reverse	ACCATCACAGTAACTTAGATCC
RT-PCR AGP21	Forward	GCAATGAAGATGAAGATGATGG
	Reverse	TCAGAAGTTGGGCTTGGAG

Supplemental References

Berendsen HJC, Postma JPM, van Gunsteren WF, DiNola A, Haak JR (1984) Molecular-dynamics with coupling to an external bath. *The Journal of Chemical Physics* 81:3684-3690

Berendsen HJC, Grigera JR, Straatsma TPJ (1987) The missing term in effective pair potentials. *The Journal of Physical Chemistry* 91:6269-6271

Bussi G, Donadio D, Parrinello MJ (2007) Canonical sampling through velocity rescaling. *The Journal of Chemical Physics* 126:014101

Chaiwanon, J., & Wang, Z.-Y. (2015). Spatiotemporal Brassinosteroid Signaling and Antagonism with Auxin Pattern Stem Cell Dynamics in Arabidopsis Roots. *Current Biology* 25(8), 1031–1042. http://doi.org/10.1016/j.cub.2015.02.046

Dilokpimol, A., Poulsen,C.P., Vereb,G., Kaneko,S., Schulz,A., and Geshi,N. (2014). Galactosyltransferases from *Arabidopsis thaliana* in the biosynthesis of type-II arabinogalactan: molecular interaction enhances enzyme activity. *BMC Plant Biol.* 14:90. doi:10.1186/1471-2229-14-90

Egelund, J., Obel, N., Ulvskov, P., Geshi, N., Pauly, M., Bacic, A., and Larsen Petersen, B. (2007). Molecular characterization of two Arabidopsis thaliana glycosyltransferase mutants, rra1 and rra2, which have a reduced residual arabinose content in a polymer tightly associated with the cellulosic wall residue. *Plant. Mol. Biol.* 64: 439–451.S12

Geshi, N., Johansen, J.N., Dilokpimol, A., Rolland, A., Belcram, K., Verger, S., et al. (2013). A galactosyltransferase acting on arabinogalactan protein glycans is essential for embryo development in Arabidopsis. *Plant J.* 76, 128–137.doi: 10.1111/tpj.12281

Gille S, Sharma V, Baidoo EE, Keasling JD, Scheller HV, Pauly M. (2013). Arabinosylation of a Yariv-precipitable cell wall polymer impacts plant growth as exemplified by the Arabidopsis glycosyltransferase mutant ray1. *Mol Plant*. 6(4):1369-1372. doi: 10.1093/mp/sst029

Hess B, Kutzner C, Van Der Spoel D, Lindahl E (2008) GROMACS 4: Algorithms for highly efficient, load- balanced, and scalable molecular simulation. *Journal of Chemical Theory and Computation* 4:435-444

Hess B, Bekker H, Berendsen H.J.C., Fraaije J.G.E.M. (1997) LINCS: A linear constraint solver for molecular simulations. *Journal of Computational Chemistry* 18:1463-1472

Houbaert A et al. (2018) POLAR-guided signaling complex assembly and localization drive asymmetric cell division. *Nature* 563(7732), 574-578

Kim T-W, et al. (2012). Brassinosteroid regulates stomatal development by GSK3-mediated inhibition of a MAPK pathway. *Nature* 482(7385), 419–422. http://doi.org/10.1038/nature10794

Kim, D.W. et al. (2006). Functional Conservation of a Root Hair Cell-Specific cis-Element in Angiosperms with Different Root Hair Distribution Patterns. *Plant Cell* 18(11), 2958–2970

Noguchi, T., Fujioka, S., Choe, S., Takatsuto, S., Yoshida, S., Yuan, H., … Tax, F. E. (1999). Brassinosteroid-Insensitive Dwarf Mutants of Arabidopsis Accumulate Brassinosteroids. *Plant Physiology* 121(3), 743–752

Pol-Fachin L, Verli H (2012) Structural glycobiology of the major allergen of Artemisia vulgaris pollen, Art v 1: O-glycosylation influence on the protein dynamics and allergenicity. *Glycobiology* 22:817-825

Saito, F., Suyama, A., Oka, T., Yoko-o, T., Matsuoka, K., Jigami, Y., and Shimma, Y. (2014). Identification of novel peptidyl serine O-galactosyltransferase gene family in plants. *J. Biol. Chem.* 30:20405–20420

241 Saito M., Kondo Y., and Fukuda H. (2018) BES1 and BZR1 redundantly promote phloem and
242 xylem differentiation. *Plant Cell Physiol.* 2018 59(3):590-600
243 Tironi IG, Sperb R, Smith PE, van Gunsteren WF (1995) A generalized reaction field method for
244 molecular-dynamics simulations. *The Journal of Chemical Physics* 102:5451-5459
245 Wang Z-Y, Nakano T, Gendron J, He J, Chen M, Vafeados D, Yang Y, Fujioka S, Yoshida S, Asami T
246 & Chory J (2002). Nuclear-Localized BZR1 Mediates Brassinosteroid-Induced Growth and
247 Feedback Suppression of Brassinosteroid Biosynthesis. *Developmental Cell* 2, 505–513.
248 doi.org/10.1016/S1534-5807(02)00153-3
249 Yan Z, Zhao J, Peng P, Chihara RK, Li J. (2009). BIN2 functions redundantly with other Arabidopsis
250 GSK3-like kinases to regulate brassinosteroid signaling. *Plant Physiology* 150:710–721. doi:
251 10.1104/pp.109.138099
252 Yin Y, Wang ZY, Mora-Garcia S, Li J, Yoshida S, Asami T, Chory J. (2002) BES1 accumulates in the
253 nucleus in response to brassinosteroids to regulate gene expression and promote stem
254 elongation. *Cell* 109(2):181-91

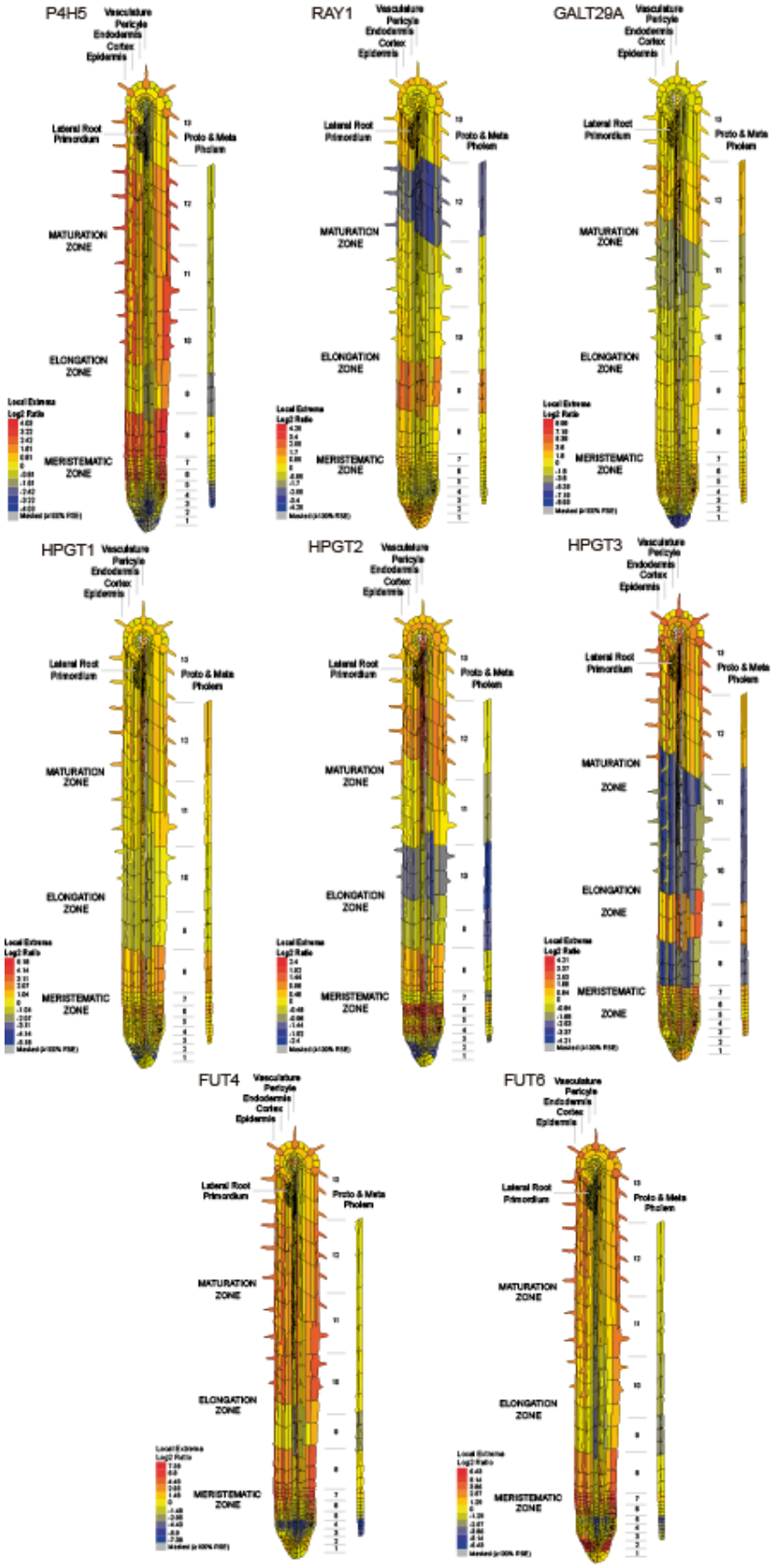
P4H5
RAY1
GALT29A
HPGT1
HPGT2
HPGT3
FUT4
FUT6
Vasculature
Pericycle
Endodermis
Cortex
Epidermis
Lateral Root Primordium
Proto & Meta Phloem
MATURATION ZONE
ELONGATION ZONE
MERISTEMATIC ZONE

256 **Supplemental Item 1. Expression pattern of enzymes involved in proline hydroxylation and *O*-**
257 **glycosylation of AGPs in the *Arabidopsis* roots.**
258 Expression of P4H5, GALT29A, RAY1, HPTG1-HPGT3 and FUT4/FUT6 are based on ePlant server
259 (http://bar.utoronto.ca/eplant/), tissue and experiments eFP viewers. Most of these AGP-
260 modifying enzymes are highly expressed in epidermal cells.

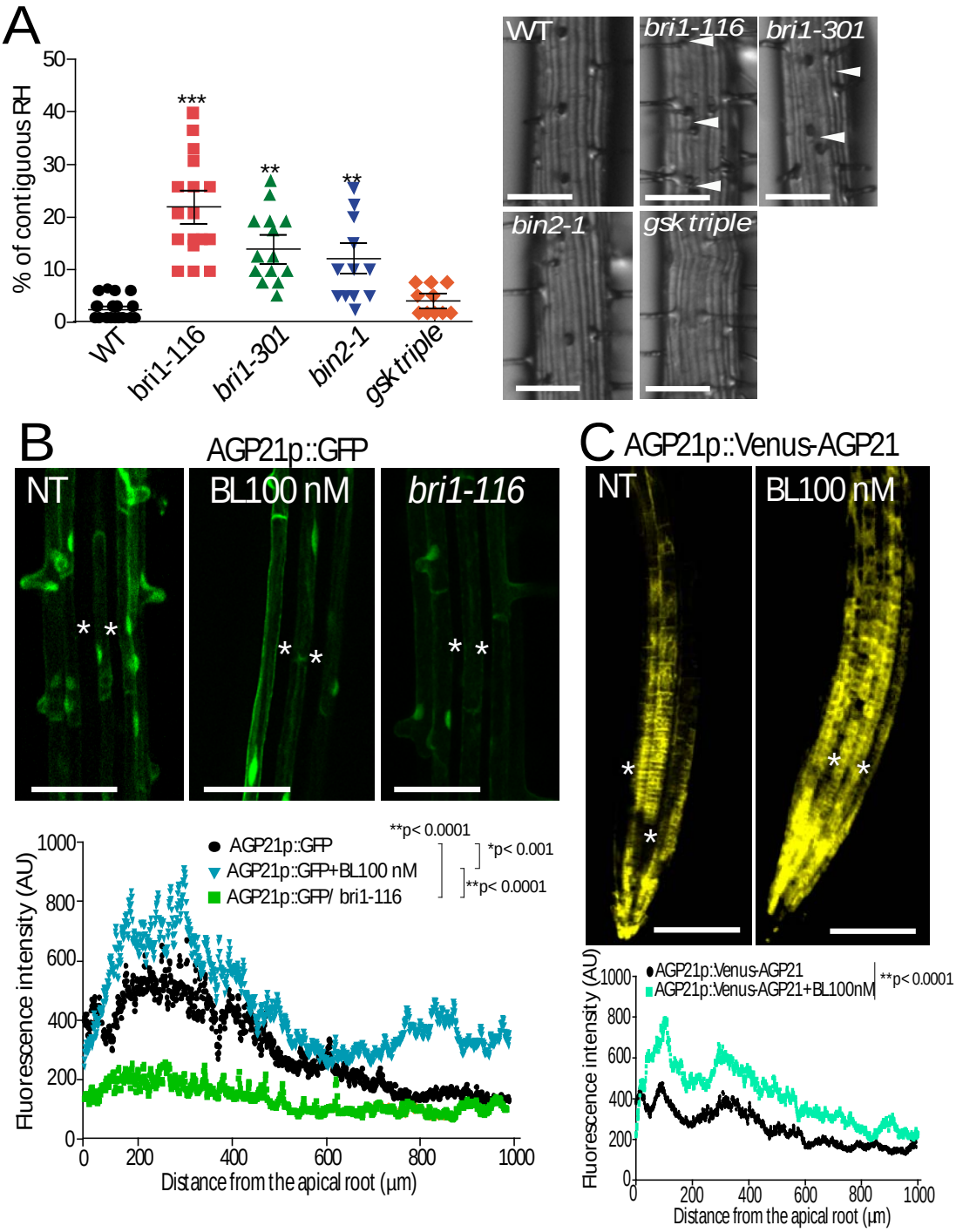

Supplemental Item 2. BR deficiency triggers RH abnormal development and BR control of AGP21 expression.

(A) Contiguous RH phenotype developed in BR constitutive active *bin2-1* and *gsk triple* (mutant mutant *bin2-3,bil1,bil2*) as well as in *bri1* mutants. Pictures indicate the RH phenotype in detail. Arrowheads indicate two contiguous RH cell protuberances. Scale bar= 50 µm. *P*-value of one-way ANOVA, (***) P<0.0001, (**) P<0.001.

270 (B) Effect of 100 mM BL (brassinolide, an active form of BR) or *bri1-116* mutation on the
271 expression of AGP21p::GFP transcriptional reporter. Quantification of V-AGP21 intensity signal is
272 indicated along the root axis in each treatment. Scale bar= 50 µm. Asterisk indicates lack of
273 expression in atrichobast cells. Scale bar= 50 µm.
274 (C) Effect of BL on the expression of the AGP21p::V-AGP21 protein reporter. Quantification of V-
275 AGP21 intensity signal is indicated along the root axis in each treatment. Scale bar= 200 µm.
276 Asterisk indicates lack of expression in atrichobast cells.

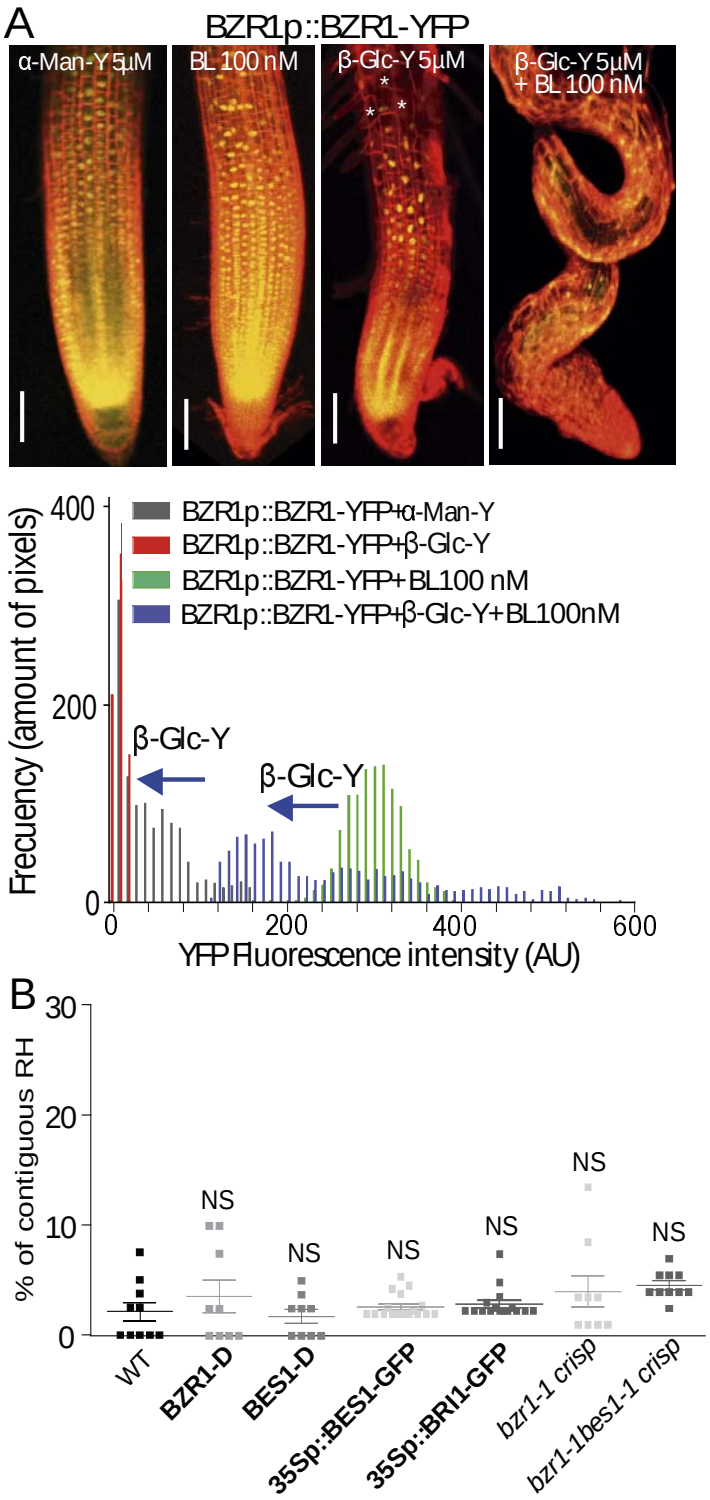

Supplemental item 3. Disruption of AGPs partially suppresses the BR-mediated BZR1 expression.

(A) β-Glc-Y supressor effect on the BL response in the roots using BZR1p::BRZ1-YFP as a reporter. Representative Root pictures of each treatment on the left. On the right, histogram of the YFP-

283 signal intensity (x-axis) quantification per pixel number (y axis). AU= Arbitrary units. Scale bar=
284 50 µm. Asterisk indicates lack of expression.
285 (B) RH phenotype in BZR1-D, BES1-D, 35Sp::BES1-GFP, 35Sp::BZR1-GFP, CRISPR-CAS *bzr1* and
286 CRISPR-CAS *bes1 bzr1*. *P*-value of one-way ANOVA, (**) P<0.001. NS= not significant differences.
287 Error bars indicate ±SD from biological replicates.

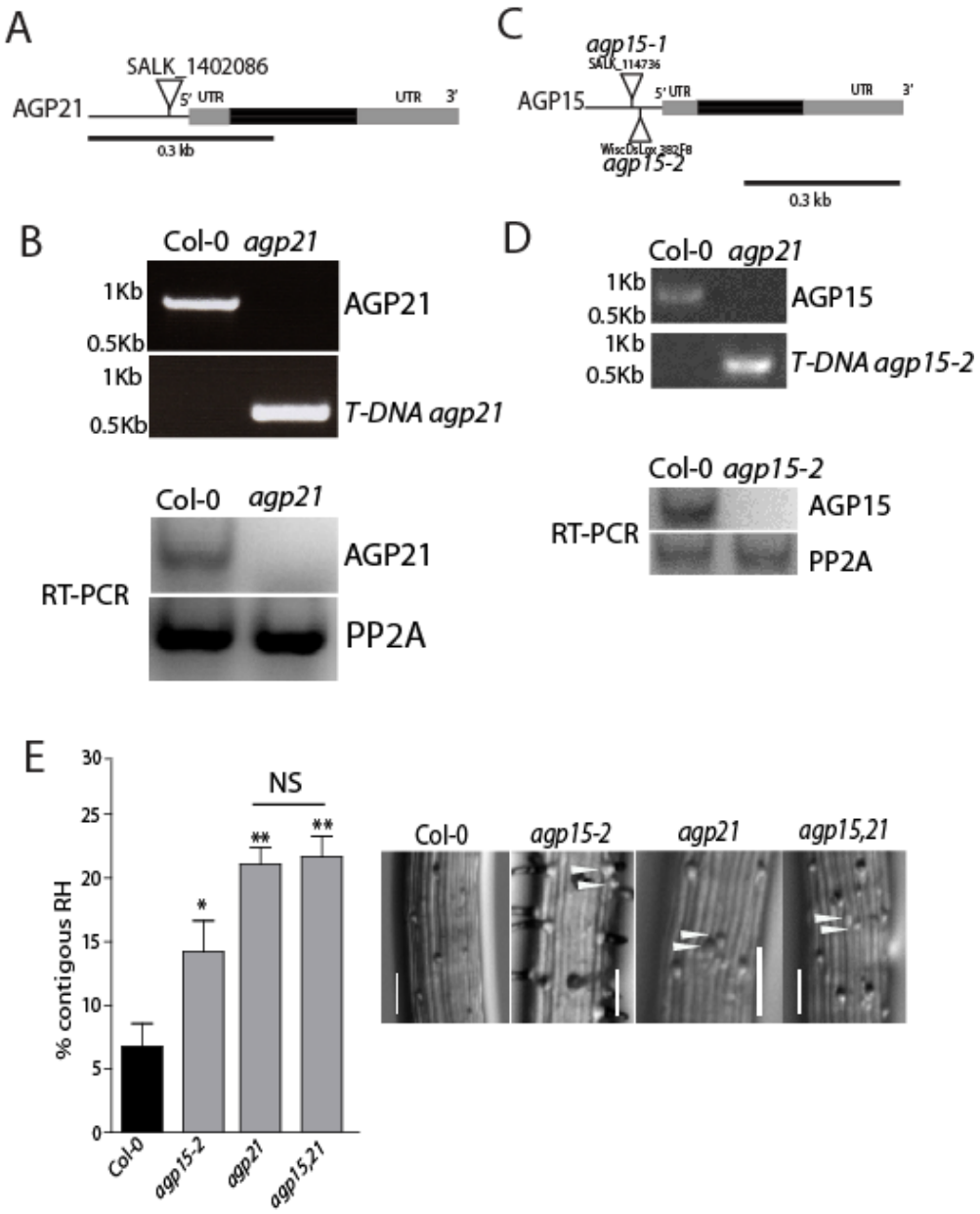

Supplemental item 4. *agp21* and *agp15* mutants characterization showed a redundant effect in RH cell fate.

(A) Schematic representation of AGP21 peptide. Position of *agp21* T-DNA insertion is indicated in the promoter region**.**

(B) Validation of *agp21* T-DNA mutant line. Total RNA was extracted from 10 days old roots. PP2A was used as control. The primers used for RT-PCR are listed in **Table S3**.

(C) Schematic representation of AGP15 peptide. Positions of T-DNA insertions are indicated. Prom: promoter region**.**

(D) Validation of *agp15* T-DNA mutant lines. Total RNA was extracted from 10 days old roots. PP2A was used as a control. The primers used for RT-PCR are listed in **Table S3**.

300 (E) Contiguous RH phenotype developed in the genetic disruption of multiple AGP peptides.
301 Pictures below each graph indicate the RH phenotype in detail. *P*-value of one-way ANOVA, (**)
302 P<0.001, (*) P<0.01. NS= not significant different. Error bars indicate ±SD from 3 biological
303 replicates. Arrowheads indicate two contiguous RH cell protuberances. Scale bar= 50 µm.
304

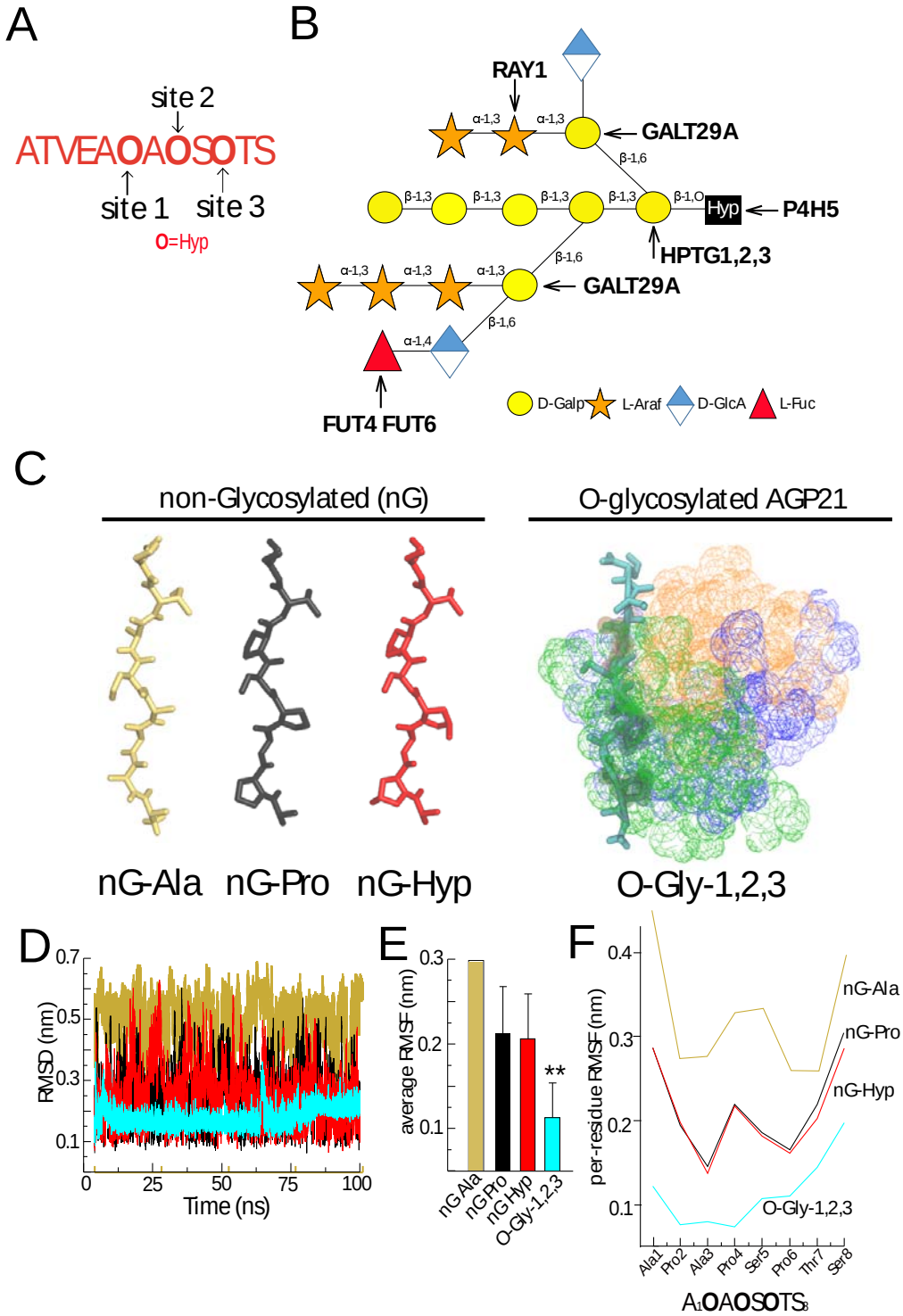

Supplemental item 5. ***O*-glycans provide stability to the AGP21 peptide conformation.**

(A) Three putative *O*-glycosylation sites present in the mature AGP21 peptide ATVEAOAOSOTS (O=Hyp).

(B) Arabinogalactan oligosaccharide (AG) composed of 15 residues including L-Glucuronic Acid (GlcA) and L-Fucose attached to each Hyp units used during MD simulations. Schematic

representation of the arabinogalactan oligosaccharide used to construct AOAOSOTS peptide glycosylated form. Mutants for some GTs used in this study (*p4h5*, triple *hpgt*, *galt29A*, *ray1* and *fut4 fut6*) are indicated.

(C) Most representative structure for the simulated glyco-peptides, in which the protein moiety is shown as sticks (with *O*-glycosylated amino acids as VDW) and the carbohydrate moieties are shown as dots. The *O*-glycan chains linked to site 1 (Hyp_2) are colored as green; to site 2 (Hyp_4) as blue; and to site 3 (Hyp_6) as orange. *O*-Gly-1,2,3 refers to a fully *O*-glycosylated AGP21 peptide.

(D) All-atom Root Mean Square Deviation (RMSD) for APAPSPTS protein moiety in the performed MD calculations.

(E) Root Mean Square Fluctuation (RMSF) obtained by averaging the per-residue values in each peptide simulation. nG abbreviates non-glycosylated; *O*-Gly-1,2,3 refers to a fully *O*-glycosylated AGP21 peptide.

(F) Per-residue RMSF for each MD condition.